FINAL REPORT OF INVESTIGATION FROM JAPANESE MAGSAT TEAM

N. Fukushima (Chairman; Geophysics Research Laboratory, University of Tokyo, Tokyo 113)
H. Maeda (Vice-Chairman; Geophysical Institute, Kyoto University, Kyoto 606)
T. Yukutake (Secretary; Earthquake Research Institute, University of Tokyo, Tokyo 113)
M. Tanaka, Y. Miyazaki (Geographical Survey Institute, Tsukuba 305)
S. Oshima (Hydrographic Department, Maritime Safety Agency, Tokyo 104)
K. Ogawa (Geological Survey of Japan, Tsukuba 305)
M. Kawamura (Magnetic Observatory, Kakioka, Ibaraki-Pref. 315-01)
S. Uyeda (Earthquake Research Institute, University of Tokyo, Tokyo 113)
K. Kobayashi (Ocean Research Institute, University of Tokyo, Tokyo 164)
M. Kono (Dept. Applied Physics, Tokyo Institute of Technology, Tokyo 152)
N. Sumitomo (College of Liberal Arts, Kyoto University, Kyoto 606)
K. Kaminuma, R. Fujii, H. Fukunishi (National Inst. of Polar Research, Tokyo 173)
T. Araki (Data Analysis Center for Geomagnetism and Spacemagnetism, Faculty of Science, Kyoto University, Kyoto 606)
A. Suzuki (College of Liberal Arts, Saga University, Saga 840)
T. Iijima (Geophysics Research Laboratory, University of Tokyo, Tokyo 113)
Y. Kamide (Department of Computer Science, Kyoto Sangyo University, Kyoto 603)
T. Saito (Geophysical Institute, Tohoku University, Sendai 980)

TITLES OF JAPANESE MAGSAT INVESTIGATIONS (Statement of Work #M-43)

A. Crustal Structure near Japan and its Antarctic Station
   - A-1. Regional Magnetic Charts
   - A-2. Local Magnetic Anomalies and Their Origin
   - A-3. Crustal Structure in the Antarctic

B. Electric Currents and Hydromagnetic Waves in the Ionosphere and the Magnetosphere
   - B-1. Ionospheric and Magnetospheric Contributions to Geomagnetic Variations
   - B-2. Field-Aligned Currents
   - B-3. Geomagnetic Pulsations and Hydromagnetic Waves

Reporting Date: March 15, 1983

Investigation Period: July 15, 1980 - November 15, 1982

(E83-10366) JAPANESE MAGSAT TEAM Final Report (Tokyo Univ.) 67 p HC A04/MF A01 CSCL 05B

N83-29777

Unclas
G3/43 00366

INTRODUCTION

1. Collaborators in Japan for MAGSAT Data Analysis

The Japanese MAGSAT Team (the initial membership is shown on the cover page) carried out investigations with MAGSAT data over the past 28 months with the assistance of the following collaborators.

I. Nakagawa (Earthquake Research Institute, University of Tokyo, Tokyo 113)
T. Nakatsuka and Y. Ono (Geological Survey of Japan, Tsukuba 305)
M. Yanagisawa (Institute of Space and Astronautical Science, Tokyo 153)
T. Kamei, T. Iyemori, S. Tsunomura and T. Kumaki (Geophysical Institute, Kyoto University, Kyoto 606)
M. Ejiri and H. Sakurai (National Institute of Polar Research, Tokyo 173)

The following persons participated in the production or analysis of ground or airborne magnetic surveys, the data of which will be fully used in the near future for comparison with MAGSAT data.

Y. Ueda, K. Onodera, T. Kaneko and F. Nakagawa (Hydrographic Department, Maritime Safety Agency, Tokyo 104)
S. Fujita (Magnetic Observatory, Kakioka, Ibaraki-Pref. 315-01)
K. Shibuya (National Institute of Polar Research, Tokyo 173)

2. Advisory Committee to the MAGSAT Team

In September 1979 an advisory committee for the MAGSAT Team was set up by the National Committee for IUGG, with the purpose of (i) giving appropriate scientific advice to the MAGSAT Team, and (ii) promoting the future possible utilization of MAGSAT data in the various disciplines beyond the subjects chosen by the MAGSAT Team for the immediate study. The MAGSAT Team welcomed the participation of the advisory members in the meetings held every four months throughout the investigation period.

3. Financial Support to the MAGSAT Team

In addition to financial support from each participating institution, the team could receive a special grant-in-aid from the Ministry of Education, Science and Culture for 1980-82, which was mainly used for (i) the meetings of the team held every four months, (ii) preparation and printing of the

Progress Reports, and (iii) reproduction and/or editing of MAGSAT data tapes for the workers in various locations in Japan. The Ministry, which endorsed the NASA-Japan cooperation of MAGSAT investigations, provided through the Institute of Space and Astronautical Science the expenses for participating in the MAGSAT Investigators' Meetings convened by NASA.

4. Research Memoranda from the Japanese MAGSAT Team Colleagues

In response to the request from the chairman of the Japanese MAGSAT Team, the team colleagues presented their research memoranda listed below.

Memo No.	Authors and Titles
A1-1	Nakagawa, I. and T. Yukutake, Spatial properties of the geomagnetic field in the area surrounding Japan.
A1-2	Ueda, Y., T. Kaneko, H. Nakagawa, K. Onodera, and S. Oshima, Evaluation of Magsat field model MGST 4/81 and the regional geomagnetic anomaly around Japan estimated from airborne magnetic survey.
A2-1	Nakatsuka, T. and Y. Ono, Geomagnetic anomalies around Japan derived from MAGSAT data.
A2-2	Nakagawa, I. and T. Yukutake, Local geomagnetic anomalies derived from MAGSAT data over the area of Japan and its surrounding seas by use of Fourier analysis technique.
A2-3	Fujita, S., M. Kawamura, T. Yukutake, Y. Ueda, T. Kaneko and S. Oshima, Regional magnetic anomaly around Japan.
A3-1	Kaminuma, K. and K. Shibuya, Aeromagnetic survey in Antarctica.
B1-1	Yanagisawa, M. and N. Fukushima, External field correction for satellite magnetic data.
B1-2	Yanagisawa, M. and N. Fukushima, Dawn/dusk asymmetry of the ring current field observed by MAGSAT.
B1-3	Yanagisawa, M. and N. Fukushima, Eastward ring current inferred from MAGSAT and OGO 5 data.
B1-4	Suzuki, A., T. Kamei, T. Kumaki and N. Fukushima, Electric current in space below the MAGSAT level.
B1-5	Maeda, H., T. Kamei, T. Iyemori and T. Araki, Geomagnetic perturbations at low latitudes observed by MAGSAT.
B1-6	Araki, T., T. Iyemori, S. Tsunomura and T. Kamei, Sudden commencements of magnetic storms observed by MAGSAT.
B2-1	Iijima, T., T. Araki and N. Fukushima, Large-scale field-aligned currents over the polar cap with reversed polarities and S_q^p associated with northward interplanetary magnetic field.

The outlines of all these memoranda are included in this Draft Final Report,

and they are cited with their Memo. No. They were first checked and summarized by T. Yukutake (for solid-earth subjects) and T. Iijima (for external magnetic field subjects) before the present Draft Final Report was written by the chairman.

We hope to publish most of the above memoranda prepared by the Japanese MAGSAT collaborators in early 1983, possibly in bulk in the "Journal of Geomagnetism and Geoelectricity", as soon as such a publication is agreed upon by NASA.

5. Additional Remarks

The following 60 pages (27 pages of text, and 33 pages of figures) is a summary of the MAGSAT investigations carried out in Japan till November 1982. In the special issue for "MAGSAT Preliminary Results (Geophysical Research Letters, Volume 9, Number 4, April 1982) the following five papers appeared as contributions from the Japanese MAGSAT Team, i.e.

Yanagisawa, M., M. Kono, T. Yukutake and N. Fukushima, Preliminary interpretation of magnetic anomalies over Japan and its surrounding area, pp. 322-324 (Paper 2L0022).

Maeda, H., T. Iyemori and T. Araki, New evidence of a meridional current system in the equatorial ionosphere, pp. 337-340 (Paper 2L0121).

Araki, T., T. Iyemori, S. Tsunomura, T. Kamei and H. Maeda, Detection of an ionospheric current for the preliminary impulse of the geomagnetic sudden commencement, pp. 341-344 (Paper 2L0157).

Suzuki, A. and N. Fukushima, Sunward or anti-sunward electric current in space below the MAGSAT level, pp. 345-347 (Paper 2L0116).

Iijima, T., N. Fukushima and R. Fujii, Transverse and parallel geomagnetic perturbations over the polar regions observed by MAGSAT, pp. 369-372 (Paper 2L0355).

The contents of these published papers are not fully reproduced in this Draft Final Report, however the important conclusions in these papers are briefly included in connection with more recent results of analyses.

In addition to the work in Japan, Y. Kamide has been cooperating with some U.S. scientists (during his stay in NOAA, Boulder, Colorado) in the comparison of MAGSAT data with other relevant data (such as electron data by TIROS-N and NOAA-6). His results are not included in this report, but they will be known later through some papers by the investigators concerned including Y. Kamide.

SUMMARY OF THE RESULTS OF MAGSAT INVESTIGATION IN JAPAN

A. CRUSTAL STRUCTURE NEAR JAPAN AND ITS ANTARCTIC STATION

The objective is to study the crustal structure near Japan and its Antarctic base by constructing a model of the regional magnetic field and investigating the local magnetic anomalies and their origin.

A-1. Regional Magnetic Charts

It has been attempted to construct a model of the regional geomagnetic field over the Japanese islands and their neighborhood for the epoch 1980.0, by means of MAGSAT data (Nakagawa and Yukutake, Memo. A1-1) and the aeromagnetic survey data obtained by the Hydrographic Department in 1980 (Ueda et al., Memo. A1-2). It was originally planned to make a model by incorporating the MAGSAT data with the surface data, with downward continuation of the MAGSAT data. Incorporation of the MACSAT data is, however, left for future work. The field synthesized by the model of the third degree polynomials was compared with the existing reference field, IGRF 1980.0 and MGST(4/81). Better agreement is seen with MGST(4/81) rather than with IGRF 1980.0 (Ueda et al., Memo. A1-2). This seems to arise from the difference in the number of terms included in the models. Poor approximation of IGRF is perhaps due to lack of terms higher than degree 10 which also represents contribution of the core field.

1. Spatial properties of the regional geomagnetic field

For the magnetically quiet period of $K_p \leq 2_o$, three component data X, Y and Z from MAGSAT Investigator-B tapes along individual paths over the area of 120°-160°E and 18°-58°N were subjected to the polynomial fit, by means of Legendre functions, by varying the maximum degree of series N from 1 to 9 (Nakagawa and Yukutake, Memo. A1-1). The study area was divided into subdivisions, 5 regions for the data of the ascending path and 5 for those of the descending path, in a strip bounded by orbital paths of every 10° intervals of longitude. Fig. A1-1 shows the decrease in the magnitude of the coefficient with the degree of the polynomial terms for the Z component along descending paths in region 8, which covers the area from the southwestern part of Japan to the east coast of Siberia. The magnitude

of the coefficient decreases rapidly from degree 1 to 6, and beyond degree 6 the rate of decrease becomes small. Similar features are seen with X and Y components and those in all other regions. If the magnitude of the coefficient is regarded as representing the amplitude spectrum, this indicates that there are two distinct structures in the spatial spectrum of the observed field. One is the lower degree terms of large amplitude, and the other is the higher degree terms of small amplitude with low decreasing rate.

The difference in the spectrum between the higher degree terms and the lower ones is more clearly seen in the residual field after removing the fitted polynomials. An example in Fig. A1-2 shows the rms residuals of the X-component plotted against the maximum degree of fitness for region 3, which covers the region from southwestern Japan to northeastern China through Korea. The rms residuals decrease sharply from degree 1 to 5, and become almost constant beyond degree 5. Similar feature are observable with the Y and Z components as well.

The above feature in the spatial spectrum is very similar to the spectrum structure obtained from the spherical harmonic analysis of the global data, suggesting that these structures are of the origin of the core and the crust respectively. The two types of field become comparable at degree 13, corresponding to the wavelength of about 3000 km (Langel and Estes, 1982).

In the present analysis, however, the overlap of the spectrum of the core and the crustal field does not always occur at the same degree. The overlap degree for the individual orbit paths was averaged in each region, and the frequency distribution of the average overlap degree in the 10 regions is shown in Fig. A1-3. For the X component, the overlap degree is either 5 or 6 in 9 regions. For the Y component the critical degree concentrates at 5. On the other hand, for the Z component it spreads toward higher harmonics up to degree 7.

From the degree of the polynomial one may roughly estimate the wavelength of the field. The degree n was related to wavelength λ by the equation

$$\lambda = L/[(n-1)/2]$$

where L is the length of the path used for the analysis, which is taken as 7000 km. The overlap degrees of 5 and 6 correspond to the wavelength

of 3500 to 2800 km. This is in agreement with the overlap wavelength 3000 km derived from the spherical harmonic analysis of worldwide data.

2. Regional magnetic charts

Aeromagnetic surveys were conducted by the Hydrographic Department of the Maritime Safety Agency in 1980 with fluxgate magnetometers for the three components (Hydrographic Department, 1982). Accuracy of the measurement was about 10 nT for the Z component, and somewhat worse for the other components, mainly controlled by the accuracy of orientation of the instrument. Total intensity was computed from the component data. Fig. A1-4 shows the flight tracks; the mean altitude of the flight was 3200 m. The surveyed data along the flight tracks were subjected to the running mean over 60 km intervals, and expanded in a polynomial series of the third degree with longitude and latitude, as

$$F, X, Y, Z = a_1 + a_2\phi' + a_3\lambda' + a_4\phi'^2 + a_5\phi'\lambda' + a_6\lambda'^2 + a_7\phi'^3 + a_8\phi'^2\lambda' + a_9\phi'\lambda'^2 + a_{10}\lambda'^3$$

where ϕ'(in radian) = ϕ(latitude)$-\phi_o$, and λ'(in radian) = λ (longitude)$-\lambda_o$, with $\phi_o = 34.0°N$ and $\lambda_o = 136.0°E$. The coefficients a_1, a_2, $\cdots\cdots a_{10}$ were determined by a least squares method so as to satisfy the conditions simultaneously $(\text{rot}\ \vec{F})_r = 0$, and $F^2 = X^2 + Y^2 + Z^2$ (Ueda et al., Memo. A1-2). The calculated coefficients are listed below.

	F	X	Y	Z
a_1	45992.93	31272.59	-3376.88	33555.50
a_2	31693.25	-24319.86	-7810.60	65319.69
a_3	-16232.68	-4586.95	3026.70	-17669.88
a_4	8583.76	-17548.71	8402.03	-29365.45
a_5	-5192.29	25466.02	-6962.53	-15106.24
a_6	-3335.83	-3732.36	15062.43	-754.07
a_7	-43638.32	28637.06	-7738.63	-32772.86
a_8	46682.60	-24573.14	5665.64	106022.66
a_9	-20867.56	7335.80	-11165.48	-38778.18
a_{10}	23507.17	-5893.14	0.0	37060.18

Figs. A1-5(a) to (d) show the computed values of F, X, Y, and Z, with the coefficients in the above table. The calculated field changes very gradually, suggesting that the major part of the field represented by the third degree polynomial model should be originated from the earth's core. If the wavelength of the field is estimated very roughly by a formula presented in a previous section, the third degree term is to represent the magnetic field wavelength of 2500 km. In terms of spherical harmonics, this corresponds to degree n=16. At this degree, the geomagnetic field observed at the surface of the earth is considered to be dominated by the crustal field. One may say that the model expressed in a third degree polynomial series represents mostly the core field, although it contains small fractions of contribution from the crustal field.

3. Comparison of the regional model with that derived from MAGSAT data

The regional field model expressed in a polynomial series was compared with MGST(4/81) model (Ueda et al., Memo. A1-2). Field values at the grid point of every 1° of longitude and latitude were synthesized from two models, the regional field model and MGST(4/81). The difference of the regional model minus MGST(4/81) is shown in Fig. A1-6 for the total intensity. The difference is small; its absolute value is less than 20 nT almost all over the Japanese islands, except for the area near the border of the surveyed area, where the difference becomes -40 nT. Comparison was also made for the vector data. Discrepancy is insignificant in the central part, less than 20 nT, for X and Z components. Regarding Y component, however, it becomes -80 nT; this large discrepancy might be caused by poorer orientation of airborne magnetometers. Hence, it may be said that, except for Y component, agreement between the regional model and MGST(4/81) is satisfactory.

Similar comparison was made with the field values computed from IGRF 1980.0. The difference is shown in Fig. A1-7 for the total intensity. Although a zero line passes through the central part of the surveyed area, the difference becomes as large as -80 nT toward the west, which is much larger than in the case of MGST(4/81).

Better approximation of the model MGST(4/81) in comparison with IGRF seems to stem from the difference in the number of spherical harmonic terms involved (up to the degree and order of 13 in MGST(4/81), and 10 in IGRF 1980.0). As was discussed earlier, the regional model contains fields with wavelengths of 2500 km, which roughly corrresponds to degree 16 in terms of the

spherical harmonic series. The IGRF 1980.0 model seems insufficient to approximate the field of this wavelength. It is perhaps due to the same reason that the past IGRF models (IGRF 1965.0 and 1975.0) have given rather poor approximation to the geomagnetic field over Japan and its vicinity.

While the past IGRF models have always given 100 to 300 nT higher values for the total intensity than observation over the area of the Japan islands, the MGST(4/81) model has been confirmed to approximate the observed field better. The field values along the flight tracks shown in Fig. A1-4 were synthesized from MGST(4/81), and then subtracted from the observed aeromagnetic data, of which running means over 18 km intervals were taken. Residuals computed in this way are shown in Fig. A1-8, where positive and negative residuals are depicted in the opposite direction from the track line. It is seen that positive and negative residuals are distributed with almost equal frequency, implying that the field value synthesized from MGST(4/81) is close to the mean field of the observed data.

A-2. Local Magnetic Anomalies and Their Origin

The objective is to extract local magnetic anomalies and to investigate their origin. There are abundant data so far accumulated by the surface surveys, not only on land, but also on the sea surface. Along with the MAGSAT data, they were originally planned to be integrated into a single data set to generate the local magnetic anomalies. For this purpose it is necessary to reduce all the data to those at a common altitude. A downward continuation program by use of a Fourier analysis technique has been completed, but not yet used practically for extraction of the short wavelength anomalies. Only the method will be described here. Accordingly, MAGSAT data were analysed independently from the surface data, and reported separately.

Two approaches were made to extract the local anomalies. The MGST (4/81) model was subtracted from the observed values, and residuals were computed (Nakatsuka and Ono, Memo. A2-1). The second approach is to apply a polynomial series approximation to a limited segment of the MAGSAT data and to compute the residuals (Nakagawa and Yukutake, Memo. A2-2). Both analyses have revealed interesting features in the crustal anomaly, but many of the detailed structures still remain unresolved. A three-dimensional Fourier analysis technique was explored with local Cartesian coordinates (Nakagawa and Yukutake, Memo. A2-2). A computer program for the downward

continuation has been tested with lower order harmonics up to 3, only giving long wavelength features.

Total intensity data in the oceanic area surrounding the Japanese islands were compiled and analysed (Fujita et al., Memo. A2-3). Data acquisition covers such a long period from 1961 to 1979, that correction of the secular variation is needed to compare the data of different epochs. Definitive International Geomagnetic Reference Field (DGRF) models were used for the correction. The analysis is still under way. The results so far obtained are consistent with those of MAGSAT analysis. The surface data reinforce new findings made only vaguely by the analysis of MAGSAT data.

Investigation of the origin of the magnetic anomalies is the most retarded part of the project. Equivalent source procedure has been employed to infer the distribution of magnetization in the crust (Yanagisawa et al., 1982). There are several factors conceivable for causing the observed magnetic anomalies. However, the preliminary study seems to suggest that either the varying thickness of the crust or its thermal structure plays an important role in generating long wavelength anomalies.

1. Local magnetic anomalies derived from MAGSAT

1-1. Anomalies as the residual field from MGST(4/81)

Anomaly maps of total intensity and vector components were drawn for the residuals of the observed field values from those computed by MGST(4/81) model (Nakatsuka and Ono, Memo. A2-1).

(a) Data selection: Only half orbit (ascending or descending) paths passing through the area in the vicinity of Japan (15°-60°N, 115°-160°E) were picked-up. In order to eliminate magnetic disturbance effect, the data for the period of $K_p \geqq 2_+$ were excluded. Attitude quality words (refer to NASA Technical Memorandum 82160) were checked and data points or poor quality in attitude ($\geqq$ 4000) were excluded.

(b) Data processing : Every orbital series of data points was tested if it had sufficiently uniform distribution in dipole latitudes, and non-uniform ones were dropped. After the subtraction of the reference field of MGST(4/81), the magnetic field data still included external (magnetospheric and ionospheric) disturbance fields. A trigonometric function form $[a \cdot \sin\phi + b \cdot \cos\phi + c]$ of dipole latitude (ϕ) was fit within the dipole latitude range of 15°-55°N, and the residual between them was assumed to

be the crustal anomaly field. This operation was applied to each component and total intensity. A statistical process is then required to draw a two-dimensional anomaly map. We take a local Cartesian coordinate system around Japan, the origin of which is located at the point of 37.5°N (geocentric), 137.5°E, and at a geocentric distance of 6800 km. In order to find mesh point value a 3-dimensional linear regression formula was applied to all data within 160 km in horizontal separations from the mesh point to be reduced, and the mesh point value at the mean elevation of these points was determined. This regression analysis was conducted at every 40 km mesh point, to get 2-dimensional mesh distribution of the magnetic field.

(c) Results: The data processing described above was applied to four kinds of data subsets, namely A(ascending dusk-side paths only, 7587 points), D (descending dawn side paths only, 10488 points), H(high-altitude paths of >6800 km geocentric distance, 9745 points) and L(Low-altitude paths of <6500 km geocentric distance, 8330 points), and the set of all available data (namely B, total of 18,075 data points). Fig. A2-1 shows the total intensity (F) anomalies around Japan extracted from each data subset A, D, H and L. Magnetic anomaly maps F,X,Y and Z extracted from set B of all available data are shown in Fig. A2-2.

(d) Discussion

We see in Fig. A2-1 that, in respect to the large scale anomaly, similar patterns are obtained irrespective of the data subset. This implies that the reproducibility of anomaly patterns of this scale is good. Also, the amplitude of anomalous field at lower altitude (d) is larger than at higher altitude (c). This result is consistent with the fact that the average elevational difference between these two data subsets is about 100 km, if we consider the crustal anomaly decreases its amplitude in proportion to the inverse square to cube of the distance.

On the other hand, there are some minor disturbances with shorter wavelength in Fig. A2-1, but they are not coincident with one another in the results from each at the data subsets. As the data processing step effectively includes a low-pass filtering operation, this process may be inadequate to reveal smaller-scale anomalies of shorter wavelength of a few hundred kilometers or less and also there may be the problem in the retrieval of the external field. Anyway, we cannot distinguish reliable magnetic anomalies.

The anomaly maps for the three components have also been made; they are more noisy than the total intensity. However, if all the available data are analysed together, the noisy character is very much reduced as seen in Fig. A2-2(b)-(d). It is concluded that the anomaly patterns with wavelengths

longer than about 500 km can be sufficiently reproduced by the present analysis.

1-2. Anomalies computed by the polynomial series

It has been confirmed that polynomial approximation for a limited area is useful to separate the crustal field from the core field (Nakagawa and Yukutake, Memo. A1-1). An anomaly map was drawn for the area of 18°-58°N and 120°-160°E, by means of the data on all the satellite paths passing through the area of 8°-68°N and 110°-170°E for the magnetically quiet period $K_{p=2_o}^{\leq}$. Since it is known that the core field becomes comparable with the crustal field at degrees from 5 to 7, the 5th degree polynomials of latitude were used to subtract the core field, and the residuals were assumed to represent the magnetic anomaly of crustal origin. Anomaly charts were drawn at an altitude of 430 km, that is an approximate mean of the satellite paths. A chart of ΔZ anomaly is shown in Fig. A2-3. Besides short wavelength anomalies, some of which are still seriously contaminated by noisy data contained in the original data set, an east-west trend of long wavelength is noticeable. Two causes are conceivable for this trend. One is the nature of the filtering process. Although the polynomial fitting process filters out the long wavelength anomalies along the orbital path, i.e. the anomalies in the north-south direction, those with a strike in the east-west direction perpendicular to the path remain unfiltered. Secondly, there is a possibility that the core field is not completely removed by the 5th degree polynomials, and that the core field contained in the 6th degree term dominates over the crustal field expressed by the rest of the polynomial series.

ΔX, ΔY and ΔZ residuals were computed into gridded values at 1.25° intervals in longitude and latitude without altitude correction, and expressed in a double Fourier series of longitude and latitude. In order to filter out the east-west trend appearing in Fig. A2-3, the first order harmonics were excluded from the series for synthesized. The results are shown in Figs. A2-4(a)-(c), where the series was synthesized up to the order of 31. It is clear in Fig. A2-4(a) that the east-west trend is almost completely removed. Instead, a weak tendency appears running in the northeast-southwest direction. It is not known at the present whether this is partly of artificial origin or not. Some are real, such as a positive belt along the Kuril islands from Kamchatka to Hokkaidô. Although there are many anomalies of short wavelength, anomalies smaller than 500 km

are supposedly artifacts created by erroneous data.

1-3. Results derived from MAGSAT data

A positive anomaly of total intensity and the vertical component seems to exist along the trench. An anomaly along the Kuril islands is particularly intense (Figs. A2-2(a) and (d), Fig. A2-4(a)), which corresponds to a narrow belt of positive anomaly observed at the surface running along the Kuril Islands on the land side of the trench. On the other hand, another positive belt that is also remarkable at the surface in the north-south direction along the east coast of Northern Honsyû is not clearly recognizable at the satellite altitude. This may suggest that the positive belt of Northern Honsyû is of shallow origin in the crust, decaying rapidly with height, while that of the Kuril Islands has deeper roots.

It is also interesting to point out that, over the Izu-Mariana trench, a positive area extends north-south (Figs. A2-2(a) and (d), Fig. A2-4(a)). This agrees well with the result of analyses of the marine data as will be discussed later, where the positive anomaly runs north-south in the west of the trench. These results seem to imply that it is a general feature of the magnetic anomaly in the subduction zone that the positive anomaly runs parallel to the trench on its island side. If this is true, it would become an important key to disclose an evolution process of the island-arc and the trench structure.

It has been believed from the surface survey that the Japan Sea is covered with a negative anomaly of ΔF and ΔZ. However, Figs. A2-2(a), (d) and Fig. A2-4(a) indicate that only the northeastern part of the Japan Sea is negative, whereas the southwestern half is rather positive. This may be related to the fact that the oceanic basin extends in the northeastern part of the Japan Sea, while in the southwestern part there are submarine rises such as the wide Yamato-tai rise. A similar feature is seen in Okhotsk Sea, where negative anomaly is more conspicuous. This seems to suggest an important nature of the back-arc basin.

Another feature to be noted is a negative anomaly of ΔZ that covers the Korean peninsula. This forms a pair with a positive anomaly in the south. In the ΔY anomaly chart of Fig. A2-4(c), we may notice a quadrant structure at the place of the pair of ΔZ anomalies, where ΔY is positive in the northeast and southwest quadrants, and negative in the northwest and southeast quadrants. These are typical patterns of the anomalies caused by dipole beneath the ground with its magnetization in the direction of the present

magnetic field. ΔX anomaly is also consistent with this model. This suggests that a highly localized magnetic material with extremely intense magnetization is buried, perhaps at a shallow depth near the southwest tip of the peninsula.

2. Three-dimensional Fourier analysis of MAGSAT data

The treatment in the previous section ignored changes in the field values caused by the change in the satellite altitude from 350 km to 500 km even on a single path. This is one of the causes generating noises that conceal the detailed structure of the anomalies. The altitude correction is an important step to refine the anomaly map.

In section A2-1-2, the field values were expanded into a Fourier series of longitude and latitude. This is a practical method when the data are given by the geodetic coordinates. However, this cannot be used for the altitude correction, because the Fourier series in longitude and latitude do not satisfy the Laplace equation in a rigorous sense.

In this section, we employed a local Cartesian coordinate system with its origin at 35°N, 140°E. The z-axis is taken vertically downwards, and the x- and y-axis toward the north and the east respectively on the plane tangent to the earth. The coordinates of the satellite position were transformed into the local coordinates, and the observed field was decomposed into X, Y and Z components or the Cartesian coordinates. The decomposed values were then subjected to a three-dimensional Fourier analysis (Nakagawa and Yukutake, Memo. A2-2).

Among the data on the paths over the area of 8°-68°N and 110°-170°E, only those with high accuracy of satellite attitude control were selected, although this process resulted in reducing the data set to about a quarter of the original size. The data thus selected were subjected to the polynomial fit. Since the core field is likely to remain in the residuals even after the trend was removed by the 5th degree series, we employed the 7th degree polynomials to compute the residual anomaly field. Of the residuals obtained in this way, those inside the space $-L/2 \leq x \leq L/2$, $-L/2 \leq y \leq L/2$ were Fourier analysed, taking the maximum order of harmonics as 3.

From the Fourier series determined in this way, it has become possible to compute the anomaly field at any point in the three-dimensional space. The anomalies at the altitude of 300 km were synthesized and are shown in Fig. A2-5. Since only the lower harmonics have been used for the analysis, the anomaly charts delineate only the long wavelength features. Upward and

downward continuation was made and the magnetic anomalies at the altitude of 100 km and 500 km were computed, of which the anomalies of the vertical component are shown in Figs. A2-6(a)and (b).

Even in this crude approximation with only the lower harmonics, one may see the magnetic features revealed in the previous section. ΔZ anomaly in Fig. A2-5, for example, shows that the northeastern part of the Japan Sea is weakly negative, while the southwestern part is positive. A positive anomaly is noticeable from the Kuril Islands to Hokkaido. A positive anomaly that runs along the Izu-Mariana trench is not well recognized in this figure. In order to see this relatively short wavelength anomaly, it is necessary to include higher harmonics in the series. On the other hand, a negative anomaly covering the Korean peninsula is very remarkable in the present case. Another feature to be mentioned is, though weak, a trend in the direction of ENE to WSW of alternating positive and negative anomalies. Further investigation is needed to confirm whether this trend is real or not.

3. Local anomalies derived from maritime data

A large amount of data has already been accumulated from the surface surveys, which can be compared with the MAGSAT data. Unfortunately, however, these surface data are not well compiled nor analysed in a form ready to compare with the satellite data except for a very few works (Nomura, 1979). Among the data accumulated in the Oceanographic Data Center of Hydrographic Department, Martitime Safety Agency, total intensity data obtained by ship-borne proton precession magnetometers covering the region of 120°E-160°E and 15°N-50°N were analyzed (Fujita et al., Memo. A2-3). The total number of data amounts to about 600,000, which had been acquired during the period from 1961 to 1979.

Since the observation covers such a long period a certain kind of correction for the geomagnetic secular variation is necessary to reduce the data to a common epoch for computing the magnetic anomalies. For the correction, we used the Definitive International Reference Field (DGRF) for 1965.0, 1970.0 and 1975.0, together with the International Geomgnetic Reference Field (IGRF) for 1980.0. In the first place, comparison was made of these reference field models with the observed fields at Japanese magnetic observatories, Memambetsu (MMB), Kakioka (KAK), and Kanoya (KNY), as shown in Fig. A2-7. The reference field values were linearly interpolated between 1965-70, 1970-75, and 1975-80. It is obvious from Fig. A2-7 that

the total intensity of the reference field is larger than that observed in Japan by about 100 nT, and the differences are almost constant for the two periods 1965-70 and 1975-80, but from 1970 to 1975 the differences increase abruptly by more than 50 nT at Memambetsu and at Kakioka. Therefore, the adopted reference field may be taken to represent the secular variation in total intensity in Japan with an accuracy of about 50 nT. Since the amplitude of magnetic anomalies in total intensity around Japan in about 300 nT, the magnetic anomaly chart based on these reference fields may not be seriously influenced by the correction of the secular variation.

The anomaly was obtained by taking the difference between the observed values and those synthesized from the reference models. At each observation point, the difference was computed, i.e. observed total intensity minus reference total intensity, and averaged every $0.25° \times 0.25°$ area. Using all the data from 1965 to 1979, Fig. A2-8 was depicted on the basis of these averaged anomalies.

For the two stable periods of the secular variation, i.e. the periods 1965-70 and 1975-80, the anomalies were computed separately and compared. Although there is a tendency that the anomalies computed from the data in 1966-70 have larger values than those in 1976-79, the general patterns of the anomalies are similar in each period. In Fig. A2-8, several features are remakable. (1) There are positive anomaly belts running parallel with trenches on their continental side, such as the anomaly along the Kuril trench, and that associated with the Japan trench, and the anomaly parallel with the Izu-Mariana trench. As has already been described, the anomalies along the Kuril trench and the Izu-Mariana trench were visible at the satellite altitude, whereas the anomaly running north-south in parallel with the Japan trench was not recognizable in the MAGSAT data. (2) The southwestern part of the Japan Sea is covered with a positive anomaly, and an area of negative anomaly spreads to the north. This feature was confirmed by the MAGSAT data. However, the marine data suggests existence of a positive area again further to the north. (3) A strong positive anomaly is clearly seen near 40°N and 155°E. This has not been confirmed by the satellite data.

On the other hand, the positive anomaly region in the Pacific Ocean marked by "?" is not clearly established. In the Pacific Ocean it is difficult to draw a clear anomaly pattern, due either to complex superposition of small scale magnetic anomalies or to sporadic distribution of the regions where data are missing. The number of data used for calculation of averaged anomaly in each unit area amounts to several hundreds near

Japan but it is only several in the Pacific Ocean far off Japan.

4. Possible causes of the magnetic anomalies

Applying an equivalent source procedure, distribution of magnetization in the earth's crust was determined to generate the observed total intensity anomalies at the MAGSAT altitude (Yanagisawa et al., 1982). In comparison with the other geophysical data, possible causes of the anomalies were investigated. Lateral variation in the thickness of the crustal layer is one possible cause. The other is difference in geothermal structure revealed by heat flow measurements. These are the most likely sources for the magnetic anomalies.

By placing magnetic dipoles at the surface of the earth with their axes parallel to the main field calculated from the MGST(4/81) model, it was attempted to interpret the anomaly of total intensity at a satellite altitude shown in Fig. A2-9, which was derived by the method described in section A2-1-1 by subtracting the MGST(4/81) field from the observation. The dipoles were placed at every 3°x3° latitude-longitude mesh points. The magnetic moment of each dipole was determined by means of an equivalent source procedure proposed by Mayhew (1979) so as to fit the observed anomaly. The magnetic moment thus obtained was then converted to a magnetization of the earth's surface layer on an assumption that the layer has a uniform thickness of 30 km. Fig. A2-10 shows the distribution of magnetization thus obtained.

A zone of high magnetization runs almost north-south near the center of the Japan Sea. Most of this high magnetization roughly coincides with the location of the Yamato-tai, a sea platform with a shallow depth of less than 2,000 m. Except for this high, the magnetization in the Japan Sea area is lower than that on the Japan Island by 1×10^{-1} to 2×10^{-1} A/m. The weak magnetization is most pronounced in the north-eastern part of the Japan Sea, i.e., most of the Japan Basin and the Yamato Basin where the depth of the bottom is typically 3,000 to 3,500 m.

Fig. A2-10 was obtained by assuming a layer of 30 km thickness for the source of magnetic anomalies. The anomalies in this figure can therefore be interpreted as representing (1) the lateral variation of susceptibility in the magnetized layer. There is however, another possibility for explaining these anomalies, i.e. (2) lateral variation of the thickness of the magnetized layer. If the thickness of the layer is assumed constant, variation of its thickness causes the magnetic anomalies. From comparison

with other geophysical data in this area, the second interpretation appears more plausible.

It was tentatively assumed that the crustal meterial had a uniform susceptibility of 4×10^{-3} in SI unit (=3.2×10^{-4}emu/cc). Then the crustal material is magnetized by 1.6×10^{-1}A/m (1.6×10^{-4}emu/cc) per unit volume under the geomagnetic field of 40 A/m (=0.5 Gauss). The magnetization contrast in Fig. A2-10, where the thickness of the layer is assumed to be a uniform 30 km, was converted to the differences of the thickness of the magnetized layer with the uniform magnetization, 1.6×10^{-1}A/m. The contrast of 1.3×10^{-1}A/m between the Japan Sea and the Japan Island in Fig. A2-10 corresponds to the 24 km difference in the thickness. This value certainly depends on the assumed susceptibility, but suggests that the magnetized layer is substantially thinner in most parts of the Japan Sea.

From the seismic data, crustal thickness is about 30 km beneath the Japan Island and about 10 km beneath the Japan Sea (Yoshii, 1979). If the Curie point isotherm is deeper than the crust/mantle boundary, the crust would be magnetized, but the mantle would not be magnetized at all (Wasilewski et al., 1979). If this is the case in this area, the thin magnetized layer in the Japan Sea may be explained by the thin crust.

On the other hand, the heat flow through the sea floor of the Japan Sea is about 100 mW/m^2, and about twice the value observed on the Japan Island (Yoshii, 1979). The Japan Sea area is characterized by low surface wave velocities, which means a hot upper mantle in this area (Abe and Kanamori, 1970). Also the large negative residual gravity anomalies indicate that the upper mantle is light and hot (Yoshii, 1972). These facts suggest that the Curie point isotherm is shallow beneath the Japan Sea and only the shallower part of the crust could be magnetized.

From the heat flow values and geothermal gradients measured at the surface, the depth of the 500°C isotherm is estimated to be about 30 km beneath the central part of Japan (Watanabe, 1968). If this can be regarded as the thickness of the magnetized layer in central Japan, the 24 km difference of the thickness leads to a 6 km magnetized layer beneath the Japan Sea. This is smaller than the Japan Sea crustal thickness (about 10 km). Therefore, this appears to suggest that the lower crust is not magnetized because of high temperature.

Study on the origin of the magnetic anomaly is still at its initial stage. Although two highly possible causes were investigated, there is no

decisive evidence to determine whether the anomaly is created by the lateral variation of the thickness of the crust or by that of the depth of the Curie point isotherm. Further investigation is needed.

A-3. Crustal Structure in the Antarctic

The ultimate goal is to clarify the crustal structure in an area near the Japanese Antarctic base stations, Syowa Station at 69°00'S, 39°35'E and Mizuho Station at 70°42'S, 49°20'E, incorporating the geomagnetic data with gravity and seismic data. The aeromagnetic survey was the central program related to the present investigation. Under severe conditions the aeromagnetic surveys were conducted and the data are now being analysed (Kaminuma and Shibuya, Memo. A3-1).

With a proton precession magnetometer, the aeromagnetic survey was intensively carried out around Syowa Station (Fig. A3-1) in 1980 and 1981. The survey was carried out along the 20 flight lines over the eastern and central part of Lützow-Holm Bay, 3 hours each, with the flight elevation of 1500 feet over the ground surface in 1980. The survey was also carried out in the Yamato Mountain area, which was located 200-300 km south from Syowa Station, and in the area between Syowa and Mizuho Stations.

Fig. A3-1 shows the course of the aeromagnetic survey at 5000 feet which was carried out in 1981 and the total flight distance was 1685 km. Surveys at 1500 feet and 3000 feet were also carried out and the total flight distance was 1120 km and 1325 km, respectively. The total intensity of the geomagnetic field for three different flight elevations of 3000, 5000 and 8000 feet is given in Fig. A3-2. These surveys were carried out along the longitude of 39°25'E from 68°50'S to 69°40'S in latitude. As the surveys were done within a few days, during a magnetically quiet period when K-index was 0-1, no correction has been made for the intensity values in Fig. A3-2.

Secular variation of the geomagnetic field at Syowa Station, is given in Fig. A3-3. The open circles indicate total intensity. The solid line indicates second-order least square regression of the observed values, where standard deviation is 37 nT. The shorter broken line gives secular variation calculated by the model IGRF(1980). The longer broken line gives similar secular variation by MGST(4/81).

Using the data obtained above, an isomagnetic chart of the total intensity is being made, and the analyses are in progress.

B. ELECTRIC CURRENTS AND HYDROMAGNETIC WAVES IN THE IONOSPHERE AND MAGNETOSPHERE

The objective is to investigate ionospheric and magnetospheric contributions to geomagnetic variations, field-aligned currents, geomagnetic pulsations and hydromagnetic waves by analysis of MAGSAT data, and if necessary also through comparison with ground magnetic variations.

B-1. Ionospheric and Magnetospheric Contributions to Geomagnetic Variations

The MAGSAT data were proved to be very useful in studying the ionospheric and magnetospheric contributions to geomagnetic field variations from various standpoints. The main results obtained so far are summarized below.

1. External field correction for satellite magnetic data

A new conventional method was introduced to learn the features of external and internal contributions to the data obtained by MAGSAT (Yanagisawa and Fukushima, Memo. B1-1). Let $\Delta\mathbf{B}$ denote the difference between the magnetic field $\mathbf{B}$ observed by MAGSAT and that given by the MGST(4/81) model. ΔX_{mag} and ΔZ_{mag} of the residual field in geomagnetic coordinates were subjected to a harmonic analysis with Legendre functions in the latitude range of $\pm 55°$, by means of the equation

$$W = a \sum_{n=1}^{6} \{E_n (\frac{r}{a})^n + I_n (\frac{a}{r})^{n+1}\} P_n(\cos\theta) \qquad (1)$$

where W is the magnetic potential for $\Delta\mathbf{B}$. The analysis was carried out for the dawn and dusk sides separately. The calculated values of external and internal coefficients (E_n and I_n) of the magnetic potential W are shown for four classes of Dst values in Fig. B1-2 with the total number of data used at the right shoulder of each diagram.

It is clear in Fig. B1-2 that E_1 increases with the absolute value of Dst, whereas E_2-E_6 are negligibly small in comparison with E_1 in all cases. This means that the magnetic field of origin external to the MAGSAT level is well approximated by a simple southward magnetic field along the geomagnetic dipole axis. A noticeable dawn/dusk asymmetry of this southward field is discussed in the next section.

The internal component of $\Delta\mathbf{B}$ consists of the induction current within the earth and the electric current flowing in the ionosphere below the

MAGSAT level. I_1 seems to increase in approximate proportion to E_1, but I_2-I_6 do not change so much with E_1 value. We may assume here that the magnetic field originated from E_1 and I_1 terms represents the ring current field and its induction effect, and the remaining fields (expecially those from I_2-I_6) the ionospheric current as a first approximation.

Fig. B1-3 shows the worldwide Z-anomaly map for (a) the dawn side and (b) the dusk side, after removing the MGST(4/81) model and the contributions from E_1 and I_1 terms. The two maps for the dawn and dusk sides differ considrably from each other because of the contamination from the ionospheric current. The latitudinal profiles of Z-anomaly in Fig. B1-3 were averaged for all longitude range, and the average is shown as delta-Z in Fig. B1-4 with standard deviations. (Fig. B1-4 confirms the peculiar latitudinal dependence of delta-Y found first by Maeda et al. (1982), but the discussion in this section is confined only to delta-Z for the dawn and dusk meridians.) The mean delta-Z curve in Fig. B1-4 is thought to represent the contribution to Z along the dawn and dusk meridians from the ionospheric current dependent on local time. Subtracting delta-Z of Fig. B1-4 from the Z-anomaly maps of Fig. B1-3, we obtain the maps shown in Fig. B1-5, in which the two maps for the dawn and dusk meridians are nearly the same as each other.

In conclusion, it is shown that the magnetospheric contribution is well represented by a simple southward field with a noticeable dawn/dusk asymmetry. The elimination of the ionospheric contributions (coming from below the MAGSAT level) gives a common anomaly map in the dawn and dusk regions.

2. Dawn-dusk asymmetry of the ring current field

The values of coefficient E_1 (which represents the southward magnetic field of magnetospheric origin) in eq. (1) of the previous section are calculated for 26 days from November 2 to 27, 1979, and shown in Fig. B1-6 (Yanagisawa and Fukushima, Memo. B1-2), together with the simultaneous Dst and Kp values. The E_1 values generally vary in close correlation with Dst, but they exhibit sometimes pronounced dawn/dusk asymmetry (enhancement at the dusk side, and a reduction at the dawn side), especially when Dst and Kp values are great. This tendency is seen in Fig. B1-7, which demonstrates that the dawn/dusk asymmetry of E_1 values is noticeable for $Kp \geq 3_-$, but almost absent for $Kp \leq 2_+$.

The quantitative relationship between E_1 and Dst values on the dawn and dusk sides is shown in Fig. B1-8 with the empirical formulae, which demonstrate the dawn-dusk asymmetry of E_1-Dst relationship but with nearly the same offset value of 22-23 nT for Dst=0.

Since the ground Dst contains also the contribution from the induced electric current within the earth, which is a main part of I_1 in eq. (1), the comparison of $E_1 + I_1$ versus Dst was also made and is shown in Fig. B1-9. From this figure we see that the average empirical formula for the dawn and dusk sides is $E_1 + I_1 = -1.0\ Dst + 24$.

A comparison of the results observed by OGO-5 (Sugiura, 1973) and MAGSAT was made to infer the ring current flow in the magnetosphere. OGO-5 observed the minimum field depression at 2.3-3.6 R_E. The empirical formulae are

$$E_1 \text{ (at OGO-5 level)} = -0.83\ Dst + 45 \text{ nT},$$

$$E_1 \text{ (at MAGSAT level)} = -0.74\ Dst + 22 \text{ nT},$$

so that $$E_1 \text{ (MAGSAT)} = 0.89\ E_1\text{(OGO)} - 18 \text{ nT}.$$

The factor 0.89 in the last equation will be attributable to the difference in geocentric distance of the observation level of MAGSAT ($\sim$1 R_E) and OGO (2.3-3.6 R_E). If we represent the ring current by a simple circular line-current, the factor 0.89 is obtained if the line current is assumed to be situated around 8 R_E. On the other hand, the difference of 18 nT between E_1(MAGSAT) and 0.89 E_1(OGO) will be reasonably attributed to an eastward ring current, which must exist in the inner edge of the westward ring current region to keep the plasma pressure of trapped charged particles in the magnetosphere. If the inner eastward current is also represented by a simple line-current at 2 R_E, the current intensity is $3 \cdot 10^5$ A, which is not an unreasonable value (Yanagisawa and Fukushima, Memo. B1-3).

3. Electric current through the plane encircled by the MAGSAT orbit

It is possible to calculate the total amount of electric current passing through the plane enclosed by the MAGSAT orbit by means of Ampère's theorem (or integrated form of a Maxwell equation) shown in Fig. B-10, where ds is a differential segment along the satellite orbit, and B_t is the magnetic field component tangential to the satellite orbit. The electric current will be reasonably thought to flow in a way shown in the figure, i.e. as field-aligned current in the magnetosphere, and as horizontal current in the ionosphere.

Attention must be paid in this analysis to the fact that MAGSAT requires 94 minutes to complete the magnetic field measurement over a complete circular path, and the earth rotates as much as 23.5° eastward under the MAGSAT orbit. This condition will result in a spurious effect on the calculated current under the MAGSAT orbit, unless the effect of the earth's rotation is corrected.

We dealt with two kinds of B_t-calculations, i.e. (a) MAGSAT orbit is fixed in the coordinate system, the earth is rotating, and (b) the earth is fixed, MAGSAT orbit plane is shifting. The calculated total current J is denoted here as (Suzuki et al., Memo. B1-4)

J(I) with MAGSAT data, and J(II) with MGST(4/81) model in case (a),

J(III) with MAGSAT data, and J(IV) with MGST(4/81) model in case (b). In the calculation in (b), the integration must be completed at the cross-point of the two successive loci of the satellite (cross-point between T_1 and T_2 in Fig. B1-11), and B_t must be taken tangential to the loci of MAGSAT orbits projected onto the earth (not parallel to the MAGSAT path in space). In a previous paper by Suzuki and Fukushima (1982), B_t was teken always tangential to the MAGSAT orbit in space, so that the results included a spurious effect due to the earth's rotation. As to J(IV), the integration is for a static magnetic field derivable from a magnetic potential, so that J(IV) must vanish theoretically. The actual result showed that the total current is less than $3 \cdot 10^5$ A on a quiet day, and such an amount can be produced from a very small error in the absolute magnetic field measurement and/or in the altitude determination of MAGSAT. For example, the accumulation of 1 nT error in the absolute value of B_t results in a total current of $4 \cdot 10^4$ A. An altitude error of only 150 m will produce a total electric current of 10^5 A.

Suzuki and Fukushima (1982) published the preliminary results of their analysis. They compared the B_t-integrations with the actual MAGSAT data and with the MGST(4/81) model field, as shown in Fig. B1-12. The both integrals showed the total current of $4 \cdot 10^6$ A in magnitude with predominant semidiurnal variation, and the difference of these two calculations was assumed to indicate the electric current in space below the MAGSAT level. However, the authors would like to revise their conclusion in this report because of criticism of the method of calculation described above.

The J(I)-J(II) calculation for a quiet day, that of November 5, 1979, in Fig. B1-13(a) in nearly the same as that of the right diagram of Fig. B1-12

(which is a reproduction from the Suzuki-Fukushima paper (1982), but with a slight correction on the previous work). This result contains a spurious effect of the earth's rotation. The apparent semi-diurnal variations of the sunward or anti-sunward electric current in space below the MAGSAT level is now understood mainly as an effect from g_2^2-term of the earth's magnetic field (a paper for this interpretation is now in preparation). The reduction of semi-diurnal amplitude in the right diagram, with actual MAGSAT data in Fig. B1-12, in comparison with the middle diagram, with the MGST(4/81) model, will be due to an induction current in the ionosphere below the MAGSAT level, which flows to reduce the effect of the earth's rotation in a conducting medium. If the ionosphere were a perfect conductor, the UT dependence of the curve in the left diagram of Fig. B1-12 should vanish.

On the other hand, in the results of the J(III) calculation in Fig. B1-13 (b) on the same day of November 5, 1979, the total intensity of space current below the MAGSAT level is much smaller, i.e. less than 10^6 A. We are continuing the calculation of J(III) for many other days during the period of the MAGSAT flight in order to find or check the dependence of sunward or anti-sunward space current below the MAGSAT level on (i) universal time, (ii) geomagnetic activity, (iii) solar wind and interplanetary magnetic field conditions, and (iv) season. At this moment, we can show only one example, that is on a disturbed day, November 13-14, 1979. As is shown in Fig. B1-14, the space current under the MAGSAT orbit is anti-sunward in the disturbed condition with its magnitude far exceeding 10^6 A in approximate proportion to the geomagnetic AE-index.

It was described in section B-1-2 that the dawn/dusk asymmetry of Dst is pronounced when the AE-index is large. Hence we may conclude that the increase in the AE-index is accompanied by both the dawn/dusk Dst-Asymmetry and the intensification of anti-sunward space current below the MAGSAT level. For the disturbed condition, a schematic picture of Fig. B1-15 will emerge, which includes a partial ring current connected with the field-aligned currents in the magnetosphere and the Pedersen current in the ionosphere. Such a current system was proposed earlier by Fukushima and Kamide (1973). Although the Hall current is more important for the auroral electrojet, it is not shown in the schematic diagram of Fig. B1-15, because the Hall current does not contribute at all to the net space current below the MAGSAT level because of its divergence-free flow within the ionosphere. It must be emphasized here that the anti-sunward Pedersen current will

contribute to the electrojet along the auroral oval, although the auroral electrojet is mainly due to the Hall current in the ionosphere.

4. Geomagnetic perturbations at low latitudes due to electric currents in the ionosphere and magnetosphere (Maeda et al., Memo. B1-5)

Fig. B1-16 shows the average perturbations (ΔH, ΔD, ΔZ and ΔF; observed value minus the MGST(4/81) model) at low latitudes between 30°N and 30°S. The difference in the observed results at dawn and dusk meridians is noteworthy, especially for ΔD, which was discussed in detail in a paper by Maeda et al. (1982). (The latitudinal profile in Fig. B1-16 is similar to that shown in Fig. B1-4, but it must be remarked that the abscissa and ordinate of the two figures are drawn in opposite sense to each other, and the period of data used is also different. Furthermore, Fig. B1-4 eliminates the contribution from the ring current effect.)

The average latitudinal profile of ΔD over 270°-320° meridians is shown in Fig. B1-17, where the contours of equal ΔD values are indicated. We notice here that the peculiar ΔD at dusk exists at altitudes lower than about 450 km centered at 8°N and 8°S in dip latitudes. There is another region of ΔD centered at dip latitude 5°N, at a height of about 500 km. If the concour lines of equal ΔD are approximately regarded as stream lines of the electric current in the ionosphere-magnetosphere, the electric current in the meridian plane flows across the geomagnetic field-lines indicated by dotted lines in Fig. B1-17.

Fig. B1-18 shows the latitudinal profile of ΔD at various longitudes and the double amplitude (ΔDn + ΔDs) is shown to be proportional to 1/B, where B is the magnetic field intensity at the dip equator. The altitude dependence of the ΔD range is shown in Fig. B1-19; the range increases with decreasing altitude, from 8 nT at 500 km to 40 nT at 300 km.

The peculiar ΔD on both sides of the magnetic equator seems to be caused by a meridional current system in the ionosphere shown in Fig. B1-20, i.e. upward at the magnetic equator. The fact that the ΔD range is proportional to 1/B (in Fig. B1-18) and to the sunspot number (in Fig. B1-21) will support the ionospheric origin of ΔD anomaly. Takeda and Maeda (in preparation) have recently carried out a calculation of F-region dynamo driven by pressure gradient in the evening, and obtained such a current system as that of Fig. B1-20. The electric currents flowing from or toward

the equator are not field-aligned but flow across the magnetic field-lines. The meridional currents in the dusk region in the F region have never been found in the past, in contrast to the detection by rockets for the noon equatorial E region.

A shift of the base line in ΔD seen in Fig. B1-16 (positive at dusk and negative at dawn) may be due to field-aligned currents from the northern (winter) hemisphere to the southern (summer) hemisphere in the evening and in the opposite sense in the morning; a numerical calculation by Takeda (1982) for a dynamo with NS-asymmetry seems to support this interpretation.

Fig. B1-22 shows the comparison of ΔH at dawn and dusk observed by MAGSAT with the ground Dst index, and Fig. B1-23 shows a good correlation between the dawn/dusk asymmetry with the AE-index. (The dawn/dusk asymmetry with geomagnetic activity was also shown in Fig. B1-6 and 7.). The dawn/dusk asymmetry of ΔH and its good correlation with the AE index seem to support the picture of current flow in the ionosphere and magnetosphere shown in Fig. B1-15, i.e. the presence of partial ring current and the contribution of anti-sunward current in the ionosphere to the auroral electrojet.

5. Sudden commencement of magnetic storms observed by MAGSAT

From the analysis of ground magnetograms, Araki (1977) inferred the presence of the following three kinds of electric currents flowing in the ionosphere during a sudden commencement (SC) of magnetic storms, i.e. (1) Westward zonal current induced by a sudden compression of the magnetosphere associated with an eastward current at the magnetopause; (2) Twin-vortex current for the preliminary reverse impulse on the ground, which will be attributable to a dusk-to-dawn electric field in the polar region; and (3) Twin-vortex type current due to a dawn-to-dusk electric field which develops after SC.

Since MAGSAT was making an accurate three-component measurement of the geomagnetic field above the ionosphere, it was expected to detect these currents flowing in the ionosphere through the comparison of MAGSAT and ground data, because the current flowing in the ionosphere produces a magnetic field in an opposite sense at the MAGSAT level and on the ground. This section describes the real existence of currents (1) and (2) reported by Araki et al. (Memo. B1-6), although it was partly published in a paper by Araki et al. (1982). Unfortunately, it was impossible to check current (3),

because the MAGSAT records suffered from high-latitude disturbances soon after the SC's concerned.

Twenty-two SC's were observed according to the Solar Geophysical Data (edited by J.V. Lincoln, published by WDC-A for STP, NOAA) during the MAGSAT observation period of November 2, 1979 - May 17, 1980, Araki et al. (Memo. B1-6) examined 21 cases of SC's out of 22 cases.

In low latitudes, MAGSAT detected SC mainly in H-component with a slightly greater amplitude (average value 1,3) in comparison with the ground SC data. In high latitudes, MAGSAT detected SC in both H- and D-components, but their amplitude is not always measurable (especially at latitudes higher than 60°) because of the contamination form polar disturbance. The larger amplitude of the H-component SC at the MAGSAT altitude to that on the ground will be due to a westward shielding current at the time of SC. The Z-component shows no significant change at the time of SC.

A detailed case study was made for two large SC's observed on November 30, 1979, at a low latitude, and on March 19, 1980, at a high latitude.

Fig. B1-24 shows the SC on November 30, 1979, observed by MAGSAT at the altitude of 550 km at 26.5°S, 30.3°W over the South Atlantic Ocean and on the ground (Hermanus in South Africa, Trelew in Argentina and its conjugate point Sam Juan in Puerto Rico). This SC showed a preliminary reverse impulse (PRI) in D-component, and MAGSAT recorded an eastward deviation with its maximum magnitude of 10 nT within 3 minutes after the SC. A worldwide equivalent overhead current-system for this PRI is drawn from the ground data in Fig. B1-25 for the northern hemisphere, assuming that the current flow is symmetric with respect to the geomagnetic equator. At Eusebio (3.9°S, 58.4°W) in Brazil (+5.6° geomag. lat.), a ground station close proximity to MAGSAT at the time of SC, the overhead current responsible for ΔD of PRI was northward. If the symmetry of the PRI current is assumed, ΔD of PRI at the ground subsatellite point of MAGSAT must have been eastward. Since a westward ΔD of PRI was observed by MAGSAT, Araki et al. (1982) concluded that the case of SC on November 30, 1979, was the first experimental evidence of the global ionospheric current-system for PRI of SC.

Another example of SC with PEI is shown in Fig. B1-26, which took place on March 19, 1980, when MAGSAT was passing over Magadan (60.0°N, 151.0°E) in east Siberia. The D-component at MAGSAT first decreased by 43 nT in about 2 minutes and recovered to the original level. A little

bit later, the H-component increased by 52 nT in about 1 minute. After 0621 UT irregular disturbances masked the SC variations. The right panel of Fig. B1-26 shows the time variation in the horizontal geomagnetic vector along the MAGSAT orbit. The horizontal geomagnetic vector deviation of the ground PI from the pre-SC level is also shown in the right panel by dashed arrows. We see clearly that the deviations above and below the ionosphere are in approximately opposite to each other. This case also supports the conclusion that PRI is caused by an ionospheric current.

B-2. Field-Aligned Currents

MAGSAT provides us with the best available data in the dawn and dusk regions to study the field-aligned current distribution, because of its accurate measurement of the three-component geomagnetic field and its flight at lower altitudes in comparison with other previous satellites. Insofar as the field-aligned currents in high latitudes are concerned, there are the following three regions of large-scale field-aligned currents, according to present knowledge, i.e.

(1) Region 1: average invariant latitude 72-78° on quiet days and 68-75° on disturbed days; current into the ionosphere on the dawn side and out of the ionosphere on the dusk side; total current $3\text{-}5\cdot10^6$ A without much influence of magnetic activity;

(2) Regions 2: invariant latitude 65-72° on quiet days and 62-68° on disturbed days, equatorial side adjacent to Region 1; current out of the ionosphere on the dawn side and into the ionosphere on the dusk side; total current $2\text{-}5\cdot10^6$ A dependent on magnetic activity; and

(3) Cusp Region: located poleward of and adjacent to Region 1 near local noon; total current $1.5\cdot10^6$ A; pattern is modified by B_y of interplanetary magnetic field.

In a previous paper by Iijima et al. (1982), they analyzed the MAGSAT record during a severe magnetic storm (November 13-14, 1979). In their analysis the MGST(4/81) model field was first subtracted from the actual MAGSAT data, and the residual was illustrated for ΔF, $\Delta B_{\parallel}$ and $\Delta\vec{B}_{\perp}$, where the latter two are the components parallel and perpendicular to the main geomagnetic field line of the MGST(4/81) model at each observation point. $\Delta\vec{B}_{\perp}$ was further decomposed into ΔD (dusk-to-dawn component) and ΔS (sunward component), or into geomagnetic north-south (ΔB^{XM}) and east-west (ΔB^{YM})

components. $\Delta B_{\prime\prime}$ is very useful in discussing the contribution from electric currents flowing in the ionosphere of enhanced electric oncductivity during magnetic storms, because the MAGSAT altitude is low enough to detect the influence of Hall current that attenuates steeply with height.

In this report a new result of analysis is described, which dealt with the field-aligned current distribution over the polar-cap region for an extremely quiet period when the interplanetary magnetic field was northward with a magnetiude as large as 5-20 nT. Such an interesting case has never been reported, so that the present report introduces new knowledge on the dependence of field-aligned current patterns on solar wind conditions.

Fig. B2-1 shows two examples of the latitudinal profile of the residueal magnetic field in the northern hemisphere on May 10, 1980. As is usual with quiet days, the locations of Regions 1 and 2 were several degrees higher in comparison with disturbed days; Region 1 currents were detected at 75.5-79.5° invariant latitude on the dawn side and at 74.9-78.4° on the dusk side. The most striking feature on this quiet day is the large perturbations observed poleward of Region 1 with a fairly large amplitude of $\Delta B_{\prime\prime}$ or ΔF. Two examples of the observed characteristics during consecutive paths of MAGSAT in Fig. B2-2 show the presence of upward current in the morning region and downward current in the afternoon region. The intensity of this field-aligned current confined to the region above 80° latitude was 1.7 times the Region 1 current intensity, and the current direction is opposite to Region 1 current. The concurrent $\Delta B_{\prime\prime}$ or ΔF observed by MAGSAT indicates the presence of a twin-vortex horizontal current confined to the polar-cap region, with an anti-sunward current over the geomagnetic pole that is opposite to the ordinary S_q^p current (Iijima et al., Memo. B2-1).

The results of analysis of ground magnetograms at 8 high-latitude stations also support the above conclusion. The overhead current arrows for the horizontal geomagnetic variation (deviation from the mean level between 2100-0300 MLT of May 10-11, 1980) in high latitudes in Fig. B2-3 clearly show the existence of a reversed S_q^p current near the geomagnetic pole. This is further confirmed by Fig. B2-4, which shows the simultaneous geomagnetic variation of ΔZ, namely positive in the region of a counter-clockwise ionospheric current, and negative in the region of a clockwise current in Fig. B2-3.

Although the occasional appearance of a reversed S_q^p current near the geomagnetic pole has been advocated by Iwasaki (1971), Maezawa (1976) and

others from a comprehensive analysis of ground magnetograms at high-latitude observatories during the period of northward interplanetary magnetic field, the case on May 10, 1980 is the first evidence for such a current in the ionosphere revealed in the MAGSAT data.

B-3. Geomagnetic Pulsations and Hydromagnetic Waves

It was planned, when the Japanese MAGSAT Team presented its proposal in February 1979, to study short-period hydromagnetic waves in the earth's environmental space through spectral analyses of geomagnetic fluctuations observed by MAGSAT and simultaneous data on the ground. However the team members for this item had to fulfil other obligations during 1980-82, so the this subject remains a task for the future. We hope, however, that a number of interesting results will come out in the near future after comparing the MAGSAT data and other simultaneous data, such as geomagnetic, VLF wave and auroral observations at various places in high latitudes.

References (except for the memoranda listed on Page 3)

Abe, K., and H. Kanamori, Mantle structure beneath the Japan Sea as revealed by surface waves, Bull. Earthq. Res. Inst., Univ. Tokyo, 48, 1011-1021 (1970).

Araki, T., Global structure of geomagnetic sudden commencement, Planet. Space Sci., 25, 373-384 (1977).

Araki, T., T. Iyemori, S. Tsunomura, T. Kamei, and H. Maeda, Detection of an ionospheric current for the preliminary impulse of the geomagnetic sudden commencement, Geophys. Res. Lett., 9, 341-344 (1982).

Fukushima, N., and Y. Kamide, Partial ring current models for worldwide geomagnetic disturbances, Rev. Geophys. Space Phys., 11, 795-853 (1973); Contribution of magnetospheric field-aligned current to geomagnetic bays and Sq fields: a comment on partial ring-current models, Radio Sci., 8, 1013-1017 (1973).

Iijima, T., N. Fukushima, and R. Fujii, Transverse and parallel geomagnetic perturbations over the polar regions observed by MAGSAT, Geophys. Res. Lett , 9, 369-372 (1982).

Iwasaki, N., Localized abnormal geomagnetic disturbance near the geomagnetic pole and simultaneous ionospheric variation, Rept. Ionos. Space Res. Japan, 25, 163-186 (1971).

Langel, R.A., and R.H. Estes, A geomagnetic field spectrum, Geophys. Res. Lett., 9, 250-253 (1982).

Maeda, H., T. Iyemori, T. Araki, and T. Kamei, New evidence of a meridional current system in the equatorial ionosphere, Geophys. Res. Lett., 9, 337-340 (1982).

Maezawa, K., Magnetospheric convection induced by the positive and negative Z components of the interplanetary magnetic field: quantitative analysis using polar cap magnetic records, J. Geophys. Res., 81, 2289-2303 (1976).

Mayhew, M.A., Inversion of satellite magnetic anomaly data, J. Geophys., 45, 119-128 (1979).

Nomura, M., Marine geomagnetic anomalies with intermediate wavelengths in the Western Pacific region, Bull. Ocean Res. Inst., Univ. Tokyo, No. 11, 42pp. (1979).

Sugiura, M., Quiet time magnetospheric field depression at 2.3 - 3.6 R_E, J. Geophys. Res., 78, 3182-3185 (1973).

Takeda, M., Three-dimensional ionospheric currents and field-aligned currents generated by asymmetric dynamo action in the ionosphere, J. Atmos. Terr. Phys., 44, 187-193 (1982).

Takeda, M., and H. Maeda, F-region dynamo in the evening, J. Atmos. Terr. Phys. (in preparation).

Suzuki, A., and N. Fukushima, Sunward or anti-sunward electric current in space below the MAGSAT level, Geophys. Res. Lett., 9, 345-347 (1982).

Wasilewski, P.J., H.H. Thomas, and M.A. Mayhew, The moho as a magnetic boundary, Geophys. Res. Lett., 6, 541-544 (1979).

Watanabe, T., Geothermal profiles across continental margins, Proc. Conductivity Anomaly Symposium, 167-182 (1968). (in Japanese)

Yanagisawa, M., M. Kono, T. Yukutake, and N. Fukushima, Preliminary interpretation of magnetic anomalies over Japan and its surrounding area, Geophys. Res. Lett., 9, 322-324 (1982).

Yoshii, T., Features of the upper mantle around Japan as inferred from gravity anomalies, J. Phys. Earth, 20, 23-34 (1972).

Yoshii, T., A detailed cross-section of the deep seismic zone beneath northeastern Honshu, Japan, Tectonophysics, 55, 349-360 (1979).

ACKNOWLEDGMENT

All the investigations described in this report have been carried out with the aid of MAGSAT data made available by NASA to the Japanese MAGSAT Team for the approved Statement of Work M-43. On behalf of the Japanese MAGSAT Team the chairman wishes to express sincere thanks to NASA for the useful MAGSAT data.

Naoshi Fukushima

March 15, 1983

Naoshi Fukushima
Chairman, Japanese MAGSAT Team

APPENDIX LIST OF MAGSAT PAPERS OF ORAL PRESENTATION

The Fourth Scientific Assembly of the International Association of Geomagnetism and Aeronomy, Edinburgh, Scotland, August 1981

M. Yanagisawa, M. Kono, T. Yukutake, and N. Fukushima, Magnetic anomalies over Japan and its surrounding area (submitted to the session on "Scientific Results from MAGSAT").

T. Iijima, N. Fukushima, and R. Fujii, Characteristics of magnetic field disturbances observed by MAGSAT (submitted to the session "General Contributions to IAGA Division III).

T. Iijima, Y. Kamide, R. Fujii, and N. Fukushima, Spatial relationship between field-aligned currents and the auroral electrojets - MAGSAT and Alaskan chain observations (submitted to the session "General contributions to IAGA Division III).

M. Maeda, T. Kamei, and T. Iyemori, Magnetic effect on Sq deduced from an analysis of MAGSAT data (submitted to the session "General Contributions to IAGA Division III, but cancelled because of the absence of the authors).

Semi-Annual Meetings of the Society of Terrestrial Magnetism and Electricity of Japan

The 68th Meeting, November 1980

H. Sakurai, M. Ejiri, T. Iijima, and N. Fukushima, Reduction of MAGSAT data and comparison with relevant geophysical data (1).

N. Fukushima, T. Iijima, R. Fujii, and H. Sakurai, Field-aligned current signatures in MAGSAT data.

M. Kono, and M. Yanagisawa, Preliminary results of MAGSAT data analysis.

H. Maeda, T. Araki, A. Suzuki, and T. Kamei, Analysis of geomagnetic variation field with MAGSAT data.

The 69th Meeting, May 1981

M. Kono, and M. Yanagisawa, Magnetic anomalies in the vicinity of Japan observed by MAGSAT.

T. Iijima, N. Fukushima, R. Fujii, and H. Sakurai, Characteristics of magnetic field variations observed by MAGSAT satellite.

Y. Kamide, T. Iijima, R. Fujii, and N. Fukushima, Simultaneous magnetic observations by MAGSAT and Alaskan chain stations.

A. Suzuki, T. Kamei, and T. Kumaki, Calculation of magnetospheric currents by means of MAGSAT data.

S. Tsunomura, T. Iyemori, H. Maeda, and T. Araki, Analysis of SC with MAGSAT data.

H. Maeda, T. Kamei, and T. Iyemori, Analysis of geomagnetic diurnal variation by means of MAGSAT data.

The 70th Meeting, October 1981

M. Kono, and M. Yanagisawa, Magnetic anomaly in the vicinity of Japan observed by MAGSAT.

A. Suzuki, T. Kamei, and T. Kumaki, Calculation of magnetospheric currents by means of MAGSAT data, II.

T. Iijima, and N. Fukushima, Characteristics of auroral disturbances and polar-cap disturbances observed by MAGSAT, and their interpretation.

H. Maeda, T. Araki, T. Kamei, and T. Iyemori, Analysis of geomagnetic diurnal variation by means of MAGSAT data, III.

The 71st Meeting, May 1982

M. Yanagisawa, and M. Kono, Corrections on external magnetic fields in the analysis of MAGSAT data.

I. Nakagawa, and T. Yukutake, Geomagnetic three-component anomalies in the vicinity of Japan obtained through the analysis of MAGSAT data.

A. Suzuki, T. Kamei, and T. Kumaki, Calculation of space current across the MAGSAT orbit (3rd report).

H. Maeda, T. Iyemori, T. Araki, and T. Kamei, One-month variation in the intensity of meridional electric current in the ionosphere detected by MAGSAT.

T. Iijima, N. Fukushima, and R. Fujii, Field-aligned currents during magnetic disturbance.

The 72nd Meeting, October 1982

I. Nakagawa, and T. Yukutake, Geomagnetic three-component anomalies in the vicinity of Japan obtained through the analysis of MAGSAT data.

T. Nakatsuka, and Y. Ono, Mapping of geomagnetic anomalies in the vicinity of Japan by means of MAGSAT data.

M. Yanagisawa, and M. Kono, Effect of ionospheric currents on geomagnetic anomaly maps by MAGSAT data.

M. Yanagisawa, Structure of magnetospheric ring-current inferred from an analysis of MAGSAT data.

A. Suzuki, T. Kamei, and T. Kumaki, Calculation of magnetospheric current across the MAGSAT orbit (4th report).

H. Maeda, T. Kamei, T. Iyemori, and T. Araki, Analysis of geomagnetic diurnal variation by means of MAGSAT data, IV.

T. Iijima, N. Fukushima, and R. Fujii, Structure of field-aligned currents and associated ionospheric currents.

Joint Symposium on MAGSAT Results and High-Sensitive Magnetometers, September 1980 and November 1981 in Sendai

N. Fukushima, International cooperative study with MAGSAT data (1980).

M. Kono, and M. Yanagisawa, Preliminary results of MAGSAT data analysis (1980).

T. Nakatsuka, K. Ogawa, and Y. Ono, Correction for altitude change on the geomagnetic total force measurement by MAGSAT: a model study (1980).

A. Suzuki, T. Kamei, and T. Kumaki, Plans for MAGSAT data analysis (1980).

H. Sakurai, M. Ejiri, R. Fujii, T. Iijima, and N. Fukushima, Reduction of MAGSAT data and some preliminary results (1980).

T. Nakatsuka, and Y. Ono, Magnetic anomaly mapping with MAGSAT data (1981).

T. Yukutake, and I. Nakagawa, Analysis of magnetic anomaly by double Fourier series (1981).

I. Nakagawa, and T. Yukutake, Magnetic anomaly in the vicinity of Japan by high-pass filter method (1981).

T. Yukutake, and S. Fujita, Reduction of observatory data to the period of MAGSAT observation (1981).

M. Yanagisawa, Crustal magnetization in the vicinity of Japan (1981).

I.J. Won, Magnetic anomaly over the American continent (1981).

N. Fukushima, Report on the MAGSAT Investigators' Meeting in Edinburgh in July 1981 (1981).

H. Maeda, T. Iyemori, T. Araki, and T. Kamei, Evidence of toroidal electric current in the equatorial ionosphere (with regard to ΔD anomaly) (1981).

T. Araki, T. Iyemori, and H. Maeda, Magnetic variation at the time of magnetic storms observed by MAGSAT (1981).

Y. Kamide, T. Iijima, N. Fukushima, D.S. Evans, and A.D. Richmond, Simultaneous observation of magnetic field by MAGSAT and precipitating particles by TIROS-NOAA satellites (1981).

T. Iijima, and N. Fukushima, Comparison of field-aligned currents between an extremely quiet day and a severely disturbed day (1981).

A. Suzuki, T. Kamei, and T. Kumaki, Study of field-aligned current with an application of Maxwell's equation (1981).

N. Fukushima, Comments on the electric current crossing the MAGSAT orbit plane (1981).

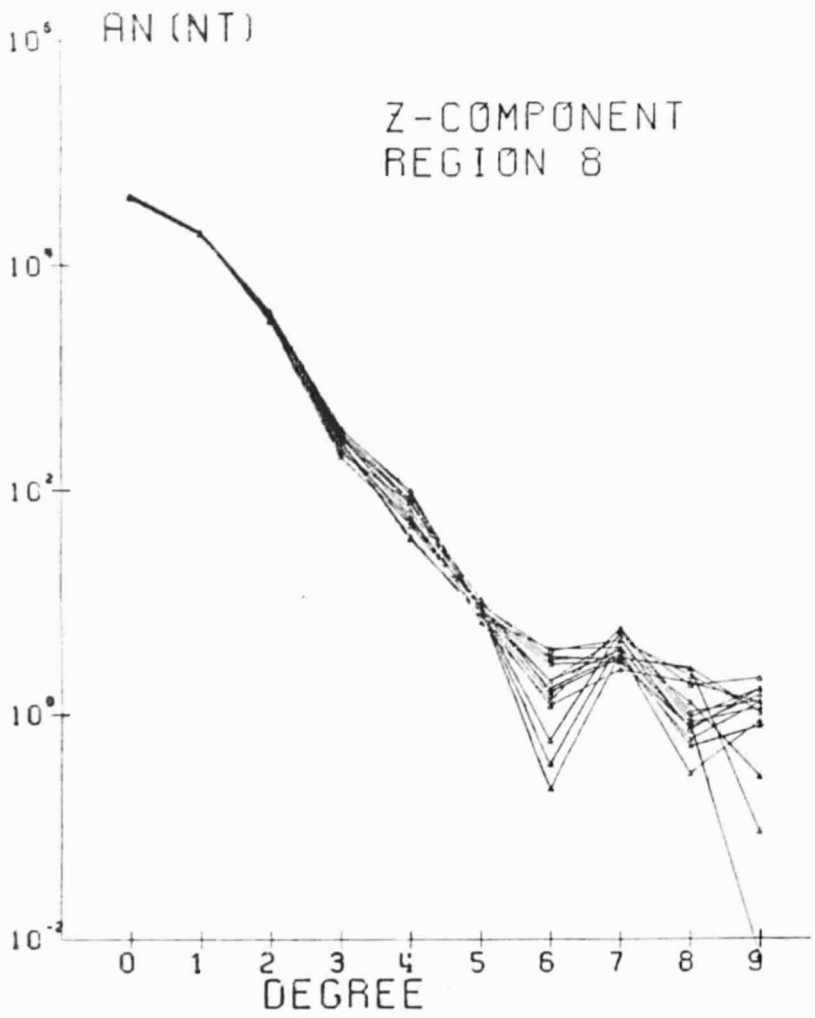

Fig. A1-1. Absolute values of the coefficients of the 9th degree polynomials determined for the Z component data along the paths in Region 8, which covers the area from the southwestern part of Japan to the east coast of Siberia.

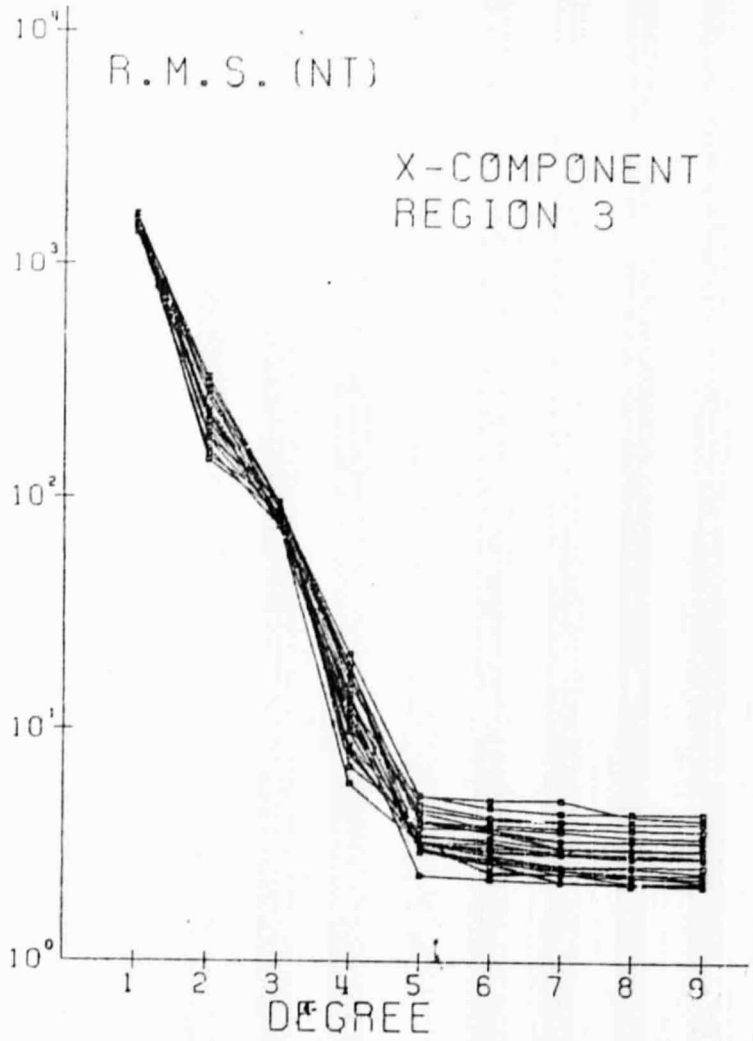

Fig. A1-2. Root mean square (R.M.S.) residuals of the X component data in the unit of nT after removal of the general trend approximated by the polynomials of latitudinal distance of degree N for Region 3, which covers the region from southwestern Japan to northeast China through Korea.

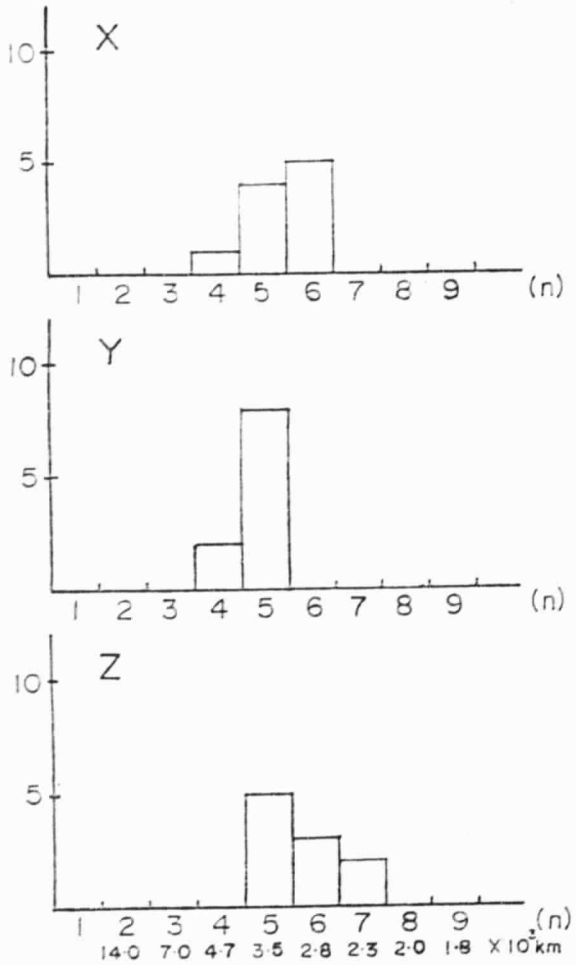

Fig. A1-3. Frequency distribution of the overlap degree at which the core field becomes comparable with the crustal field.

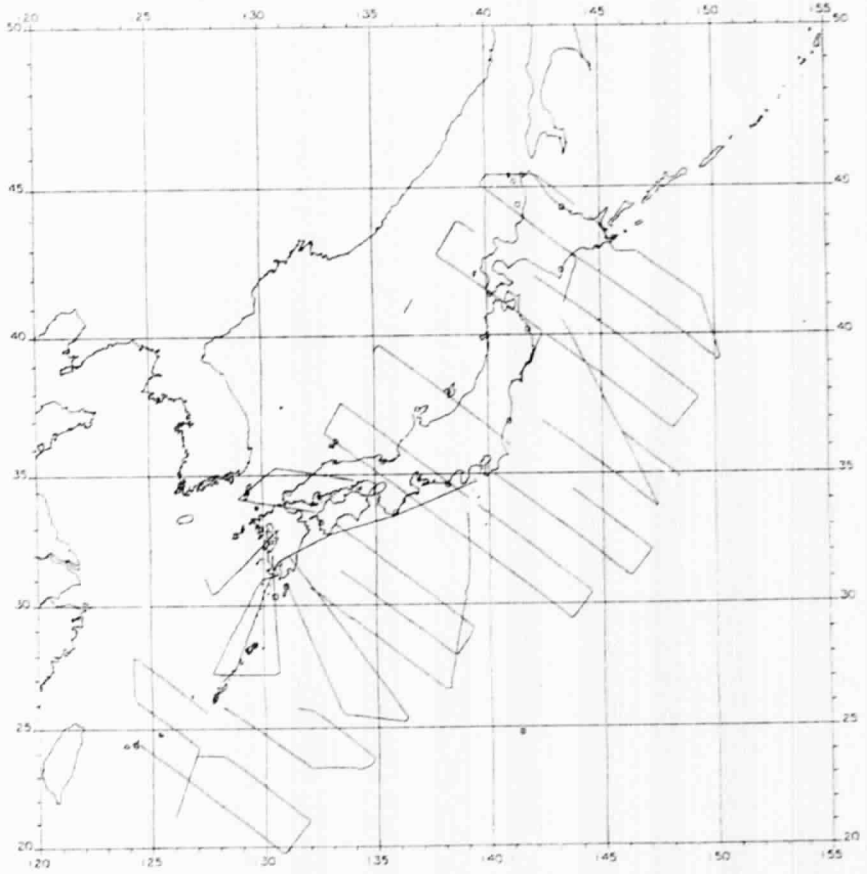

Fig. A1-4. Flight tracks of aeromagnetic surveys carried out by the Hydrographic Department, Maritime Safety Agency in 1980.

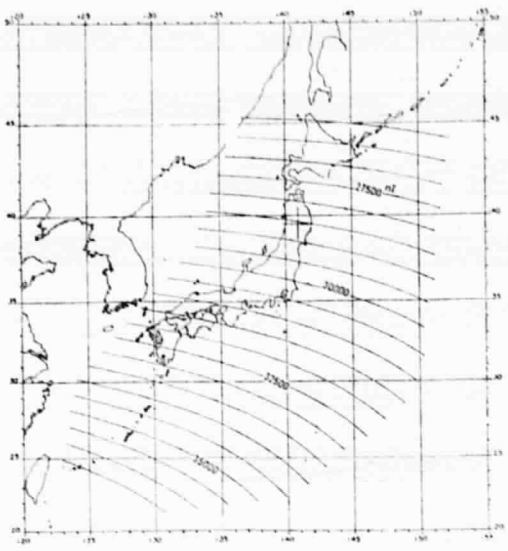

(a) X-component

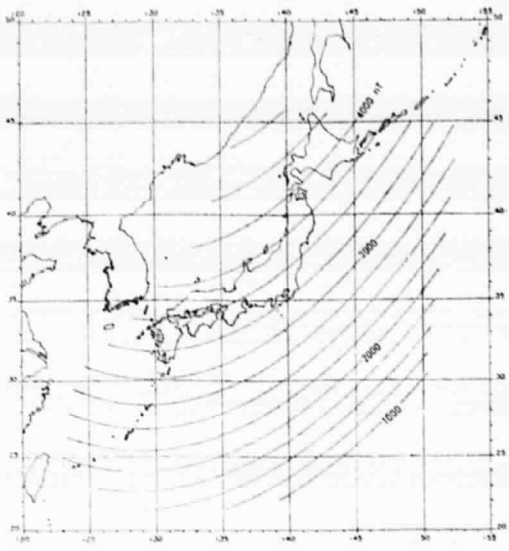

(b) Y-component

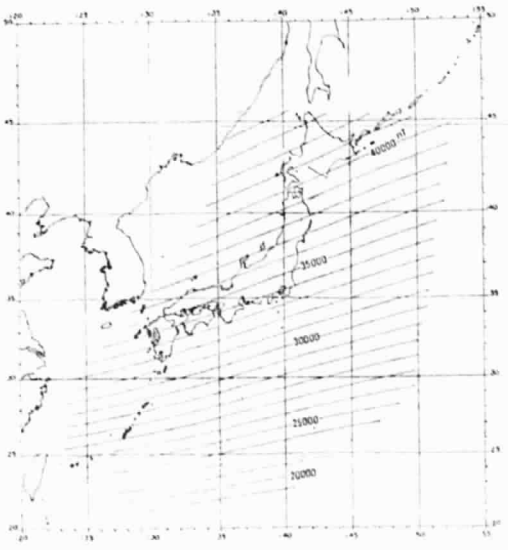

(c) Z-component

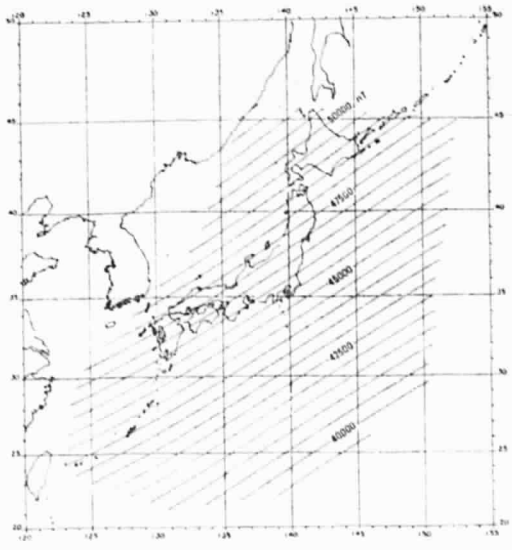

(d) total intensity F

Fig. A1-5(a)-(d). Regional magnetic chart of X, Y, Z, and F for the epoch of 1980.

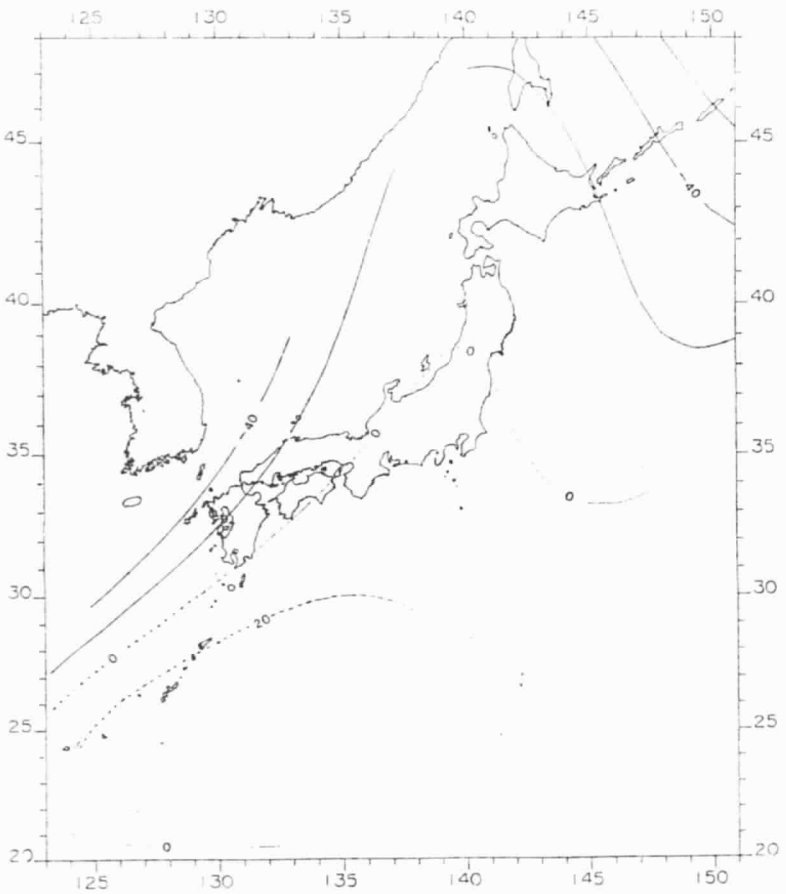

Fig. A1-6. Residuals of the geomagnetic total intensi 3rd degree polynomials — MGST (4/81) model.

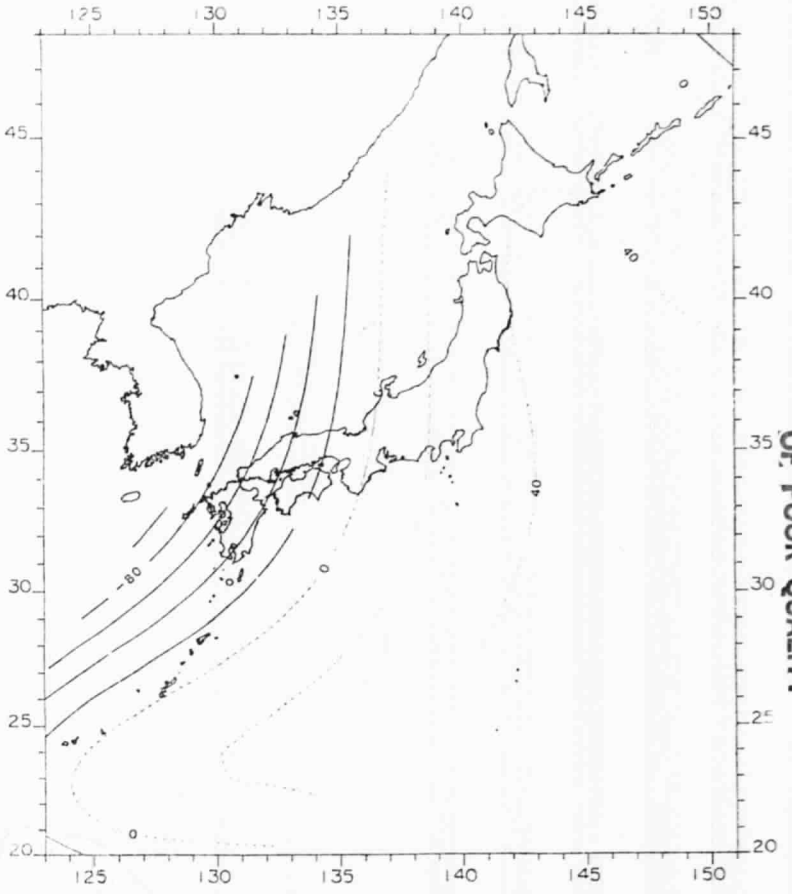

Fig. A1-7. Residuals of the geomagnetic total intensity: 3rd degree polynomials — IGRF 1980.0.

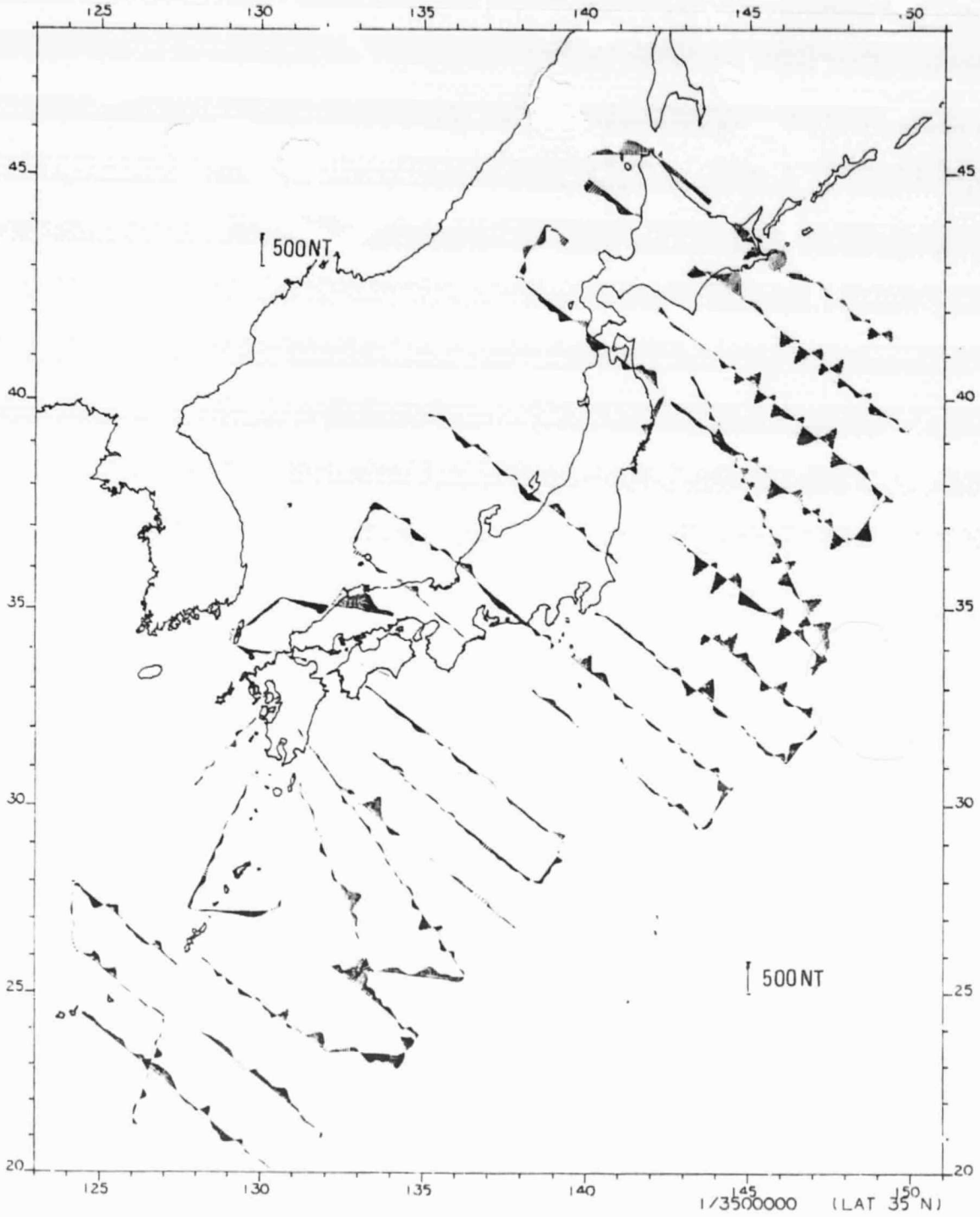

Fig. A1-8. Geomagnetic anomaly profile of total intensity. Deviations of the observed values from MGST(4/81) model.

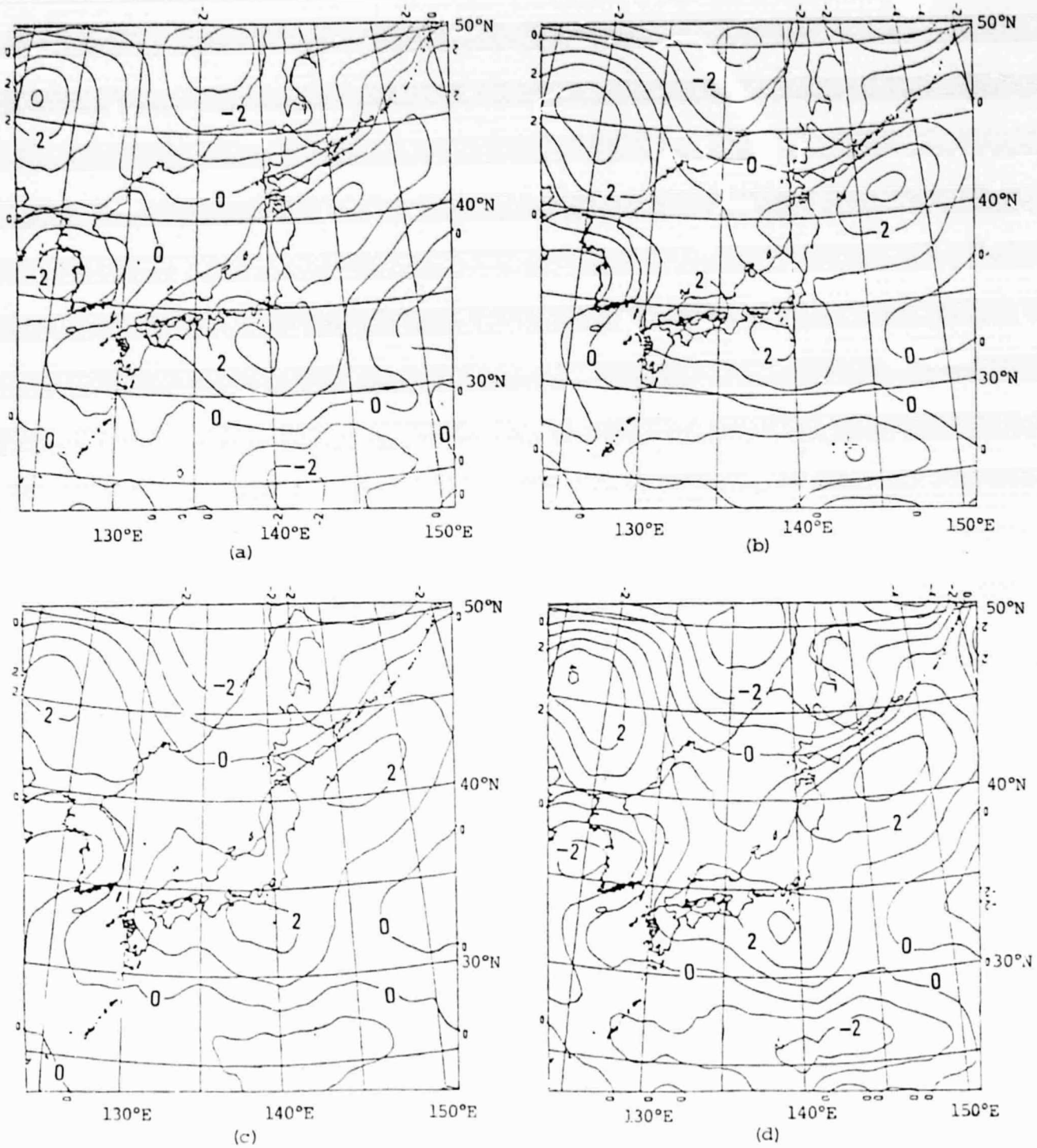

Fig. A2-1 Magnetic anomalies of total intensity (F) around Japan extracted from different data sets; i.e. (a) data subset A (ascending paths only), (b) data subset D (descending paths only), (c) data subset H (high altitude paths), and (d) data subset L (low altitude paths). Contour interval is 1 nT.

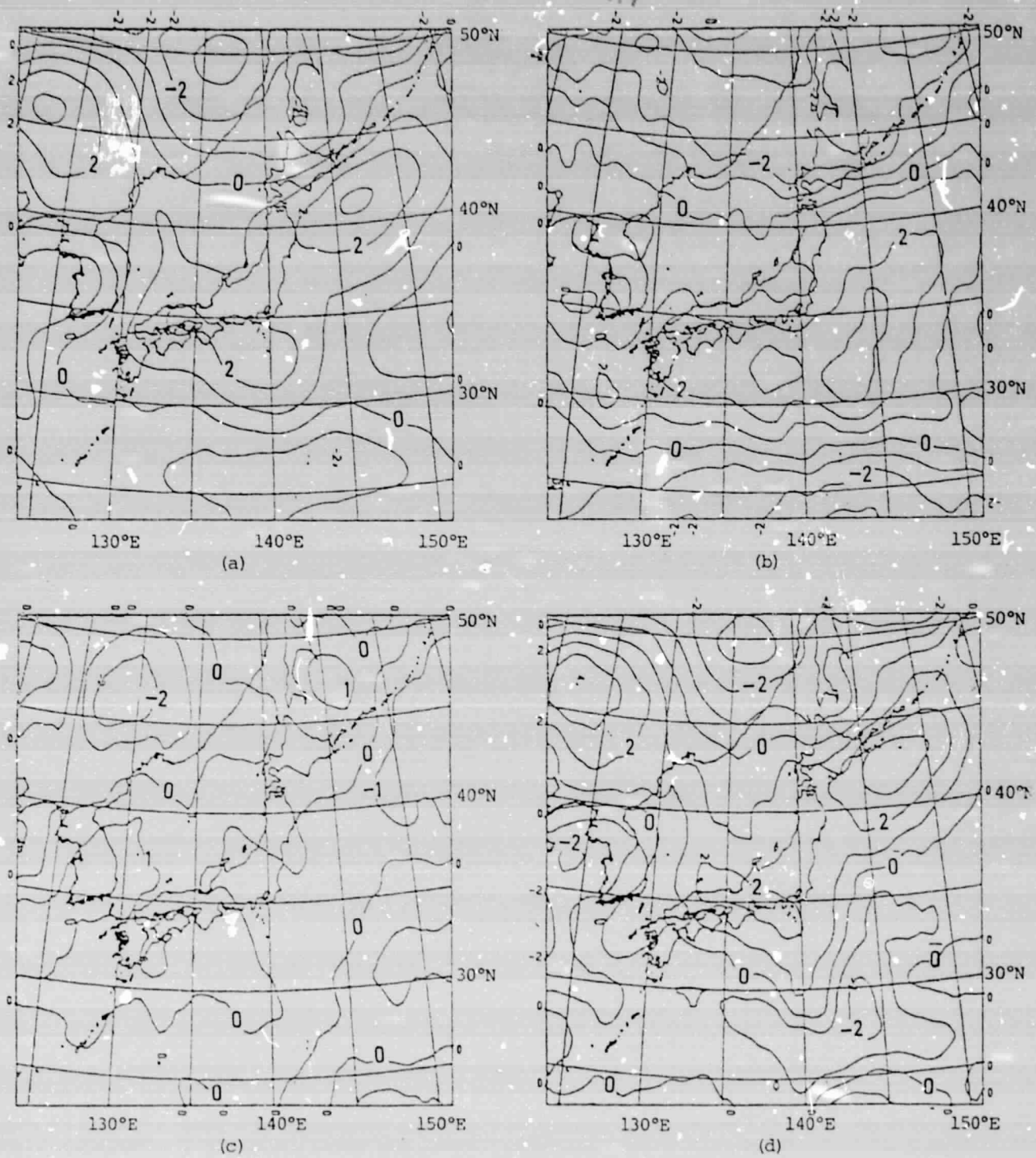

Fig. A2-2. Magnetic anomaly maps for respective components extracted from all the available MAGSAT data, for (a) total intensity, F, (b) northward component, X, (c) eastward component, Y, and (d) downward component, Z. Contour intervals are all 1 nT.

Fig. A2-3. ΔZ residuals after removal of the general trend approximated by the 5th degree polynomials. Shaded area indicates positive anomaly. Contour interval is 1 nT.

Fig. A2-4(a). Magnetic anomaly ΔZ synthesized from Fourier series with the first harmonic excluded. Shaded area indicates positive anomaly. Contour interval is 1 nT

Fig. A2-4(b). Magnetic anomaly ΔX synthesized from Fourier series with the first harmonics excluded. Shaded area indicates positive anomaly. Contour interval is 1 nT.

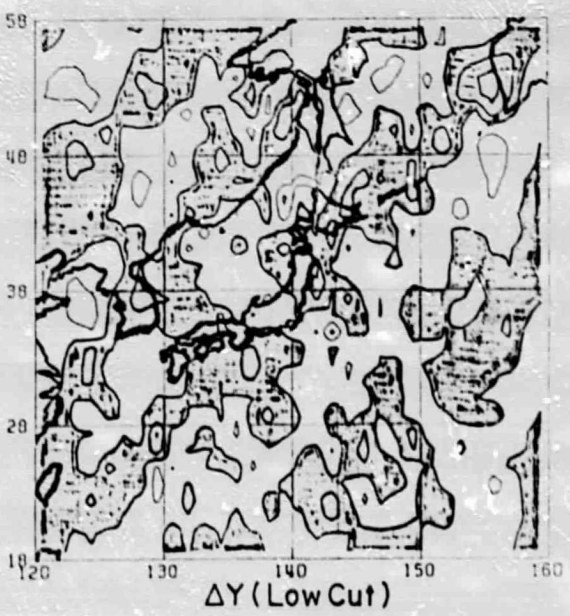

Fig. A2-4(c). Magnetic anomaly ΔY synthesized from Fourier series with the first harmonics excluded Shaded area indicates positive anomaly. Contour interval is 1 n

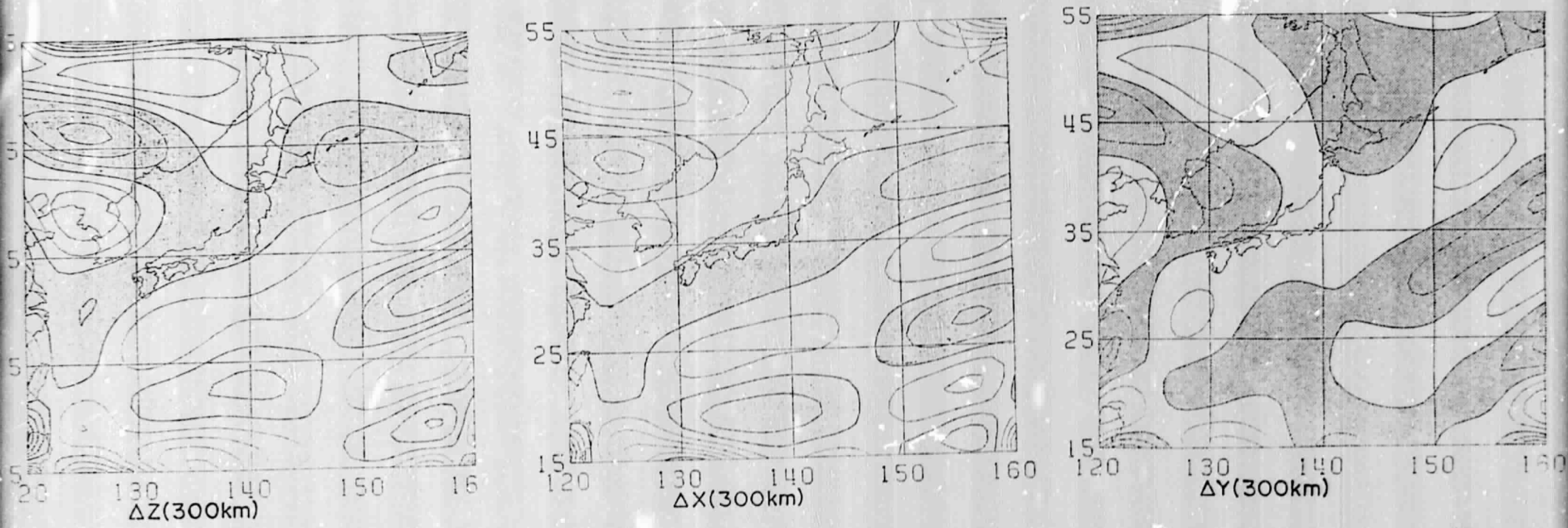

Fig. A2-5. Magnetic anomalies of ΔZ, ΔX, and ΔY at the altitude of 300 km obtained by the three-dimensional Fourier analysis. Shaded area indicates positive anomaly. Contour interval is 1 nT.

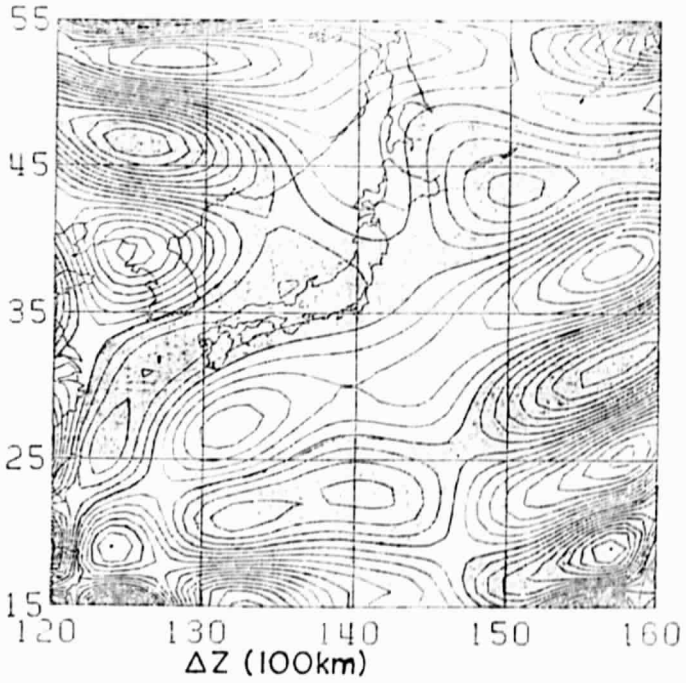

Fig. A2-6(a). ΔZ anomaly at the altitude of 100 km synthesized from a three dimensional Fourier series. Shaded area indicates positive anomaly. Contour interval is 1 nT.

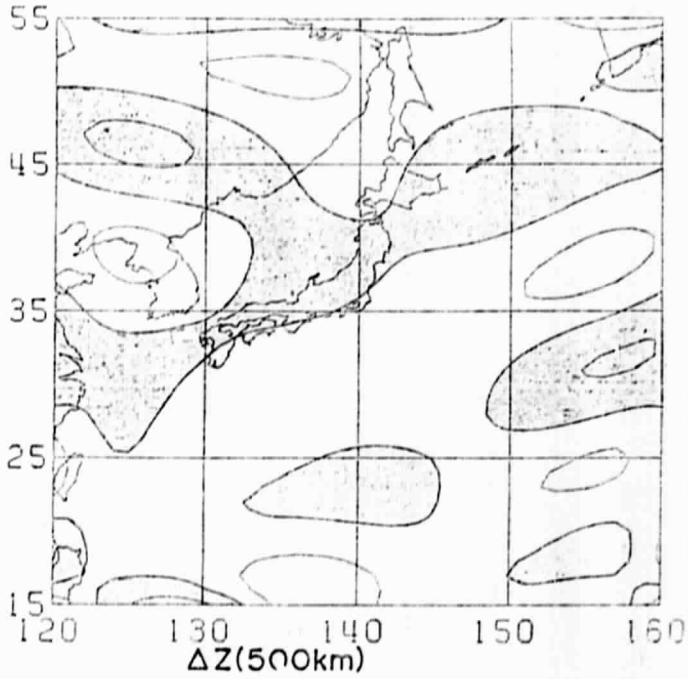

Fig. A2-6(b). ΔZ anomaly at the altitude of 500 km synthesized from a three dimensional Fourier series. Shaded area indicates positive anomaly. Contour interval is 1 nT.

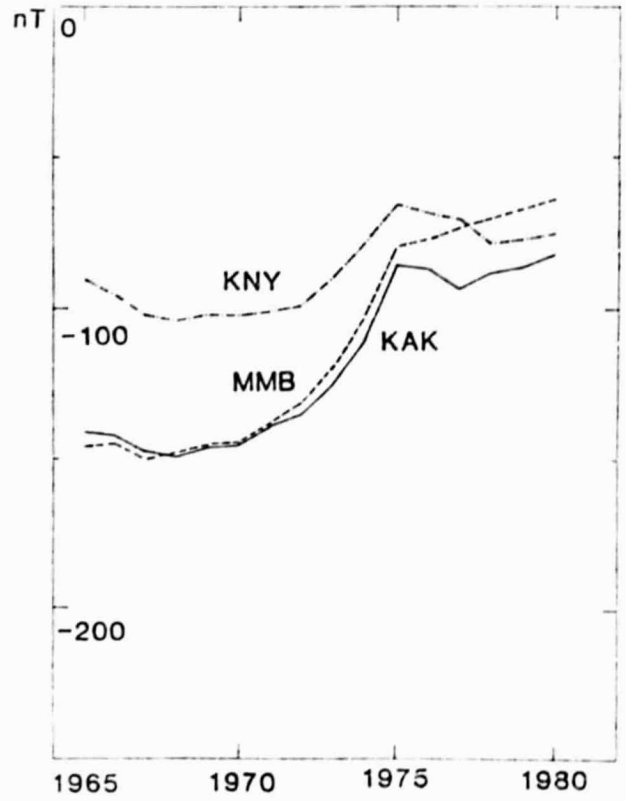

Fig. A2-7. Differences in the total intensity between the observed and the computed values from the reference field models at observatories Memambetsu (MMB: 43° 54'30"N, 144°11'35"E), Kakioka (KAK: 36°13'45"N, 140°11'23"E), and Kanoya (KNY: 31°25'14"N, 130°52'56"E).

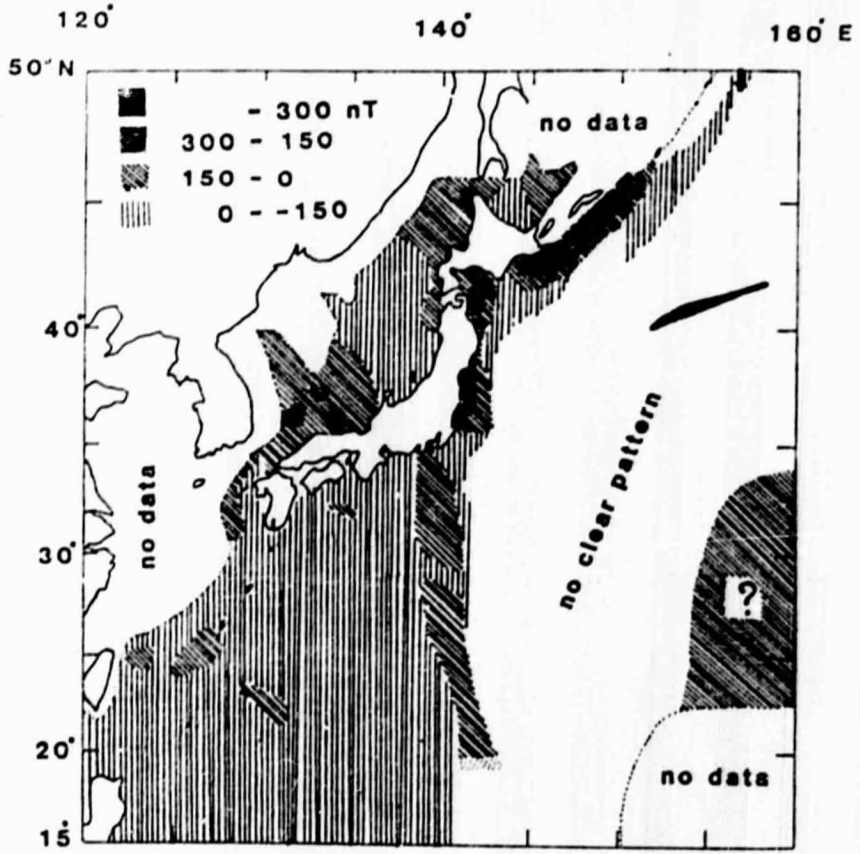

Fig. A2-8. Magnetic anomaly of total intensity obtained from the marine data for the period from 1965 to 1979. Models used are DGRF 1965, DGRF 1970, DGRF 1975 and IGRF 1980.

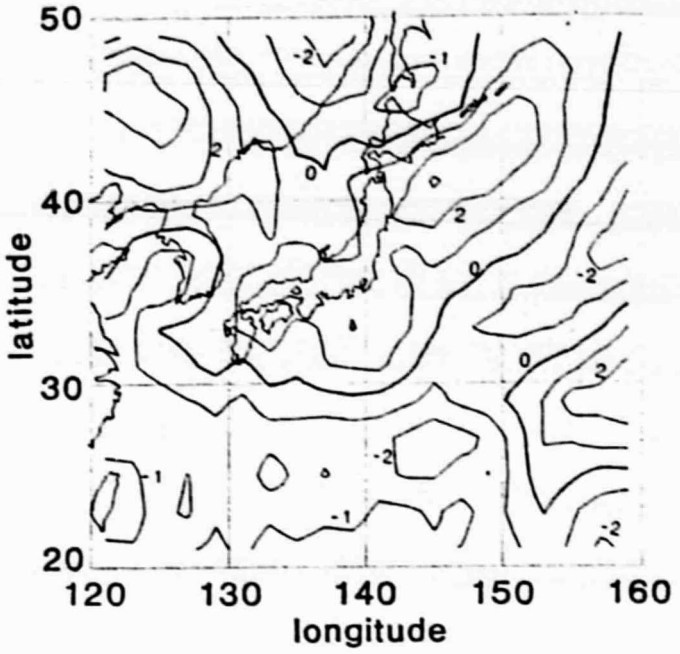

Fig. A2-9. Magnetic anomaly of total intensity (in nT) at the average altitude of 450 km.

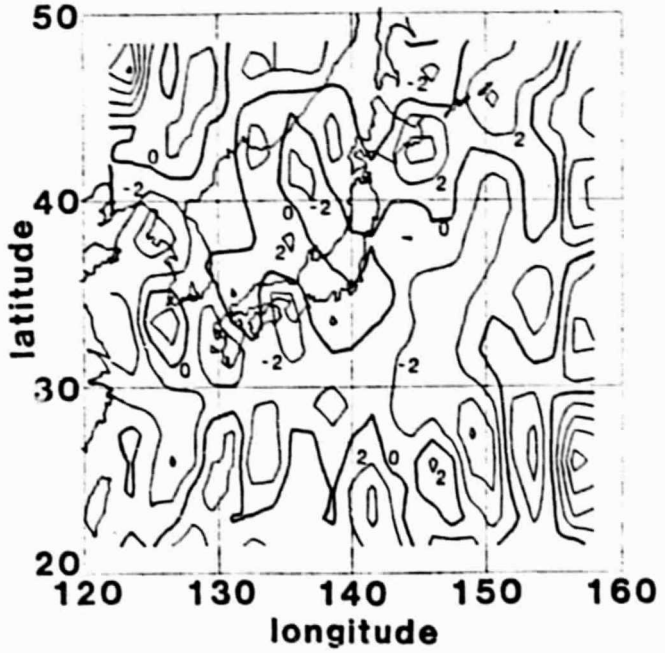

Fig. A2-10. Distribution of magnetization (in the unit of 10^{-1} A/m or 10^{-4} emu/cc) computed from the magnetic anomalies of total intensity in Fig. A2-9 by use of an equivalent source technique.

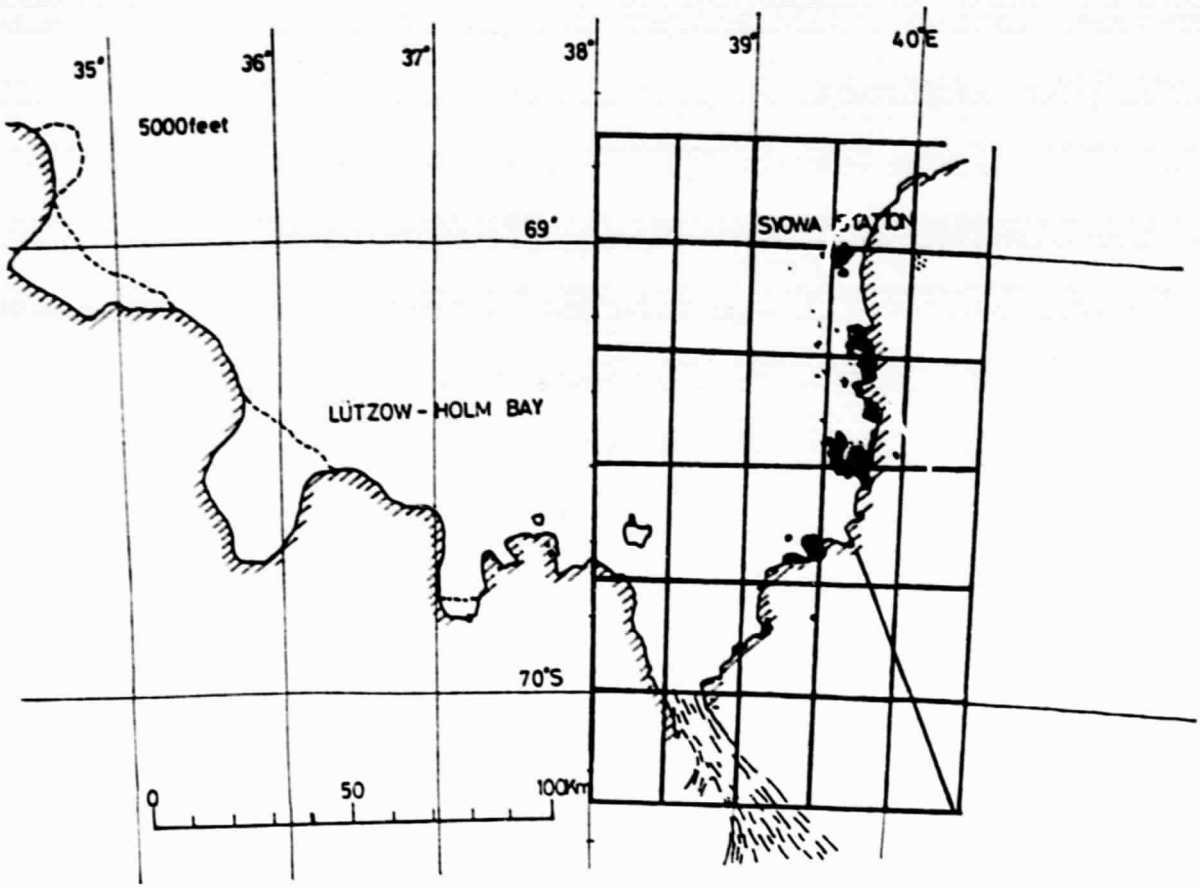

Fig. A3-1. Geographical map around Syowa Station. Thick lines indicates flight lines of aeromagnetic survey conducted in 1981.

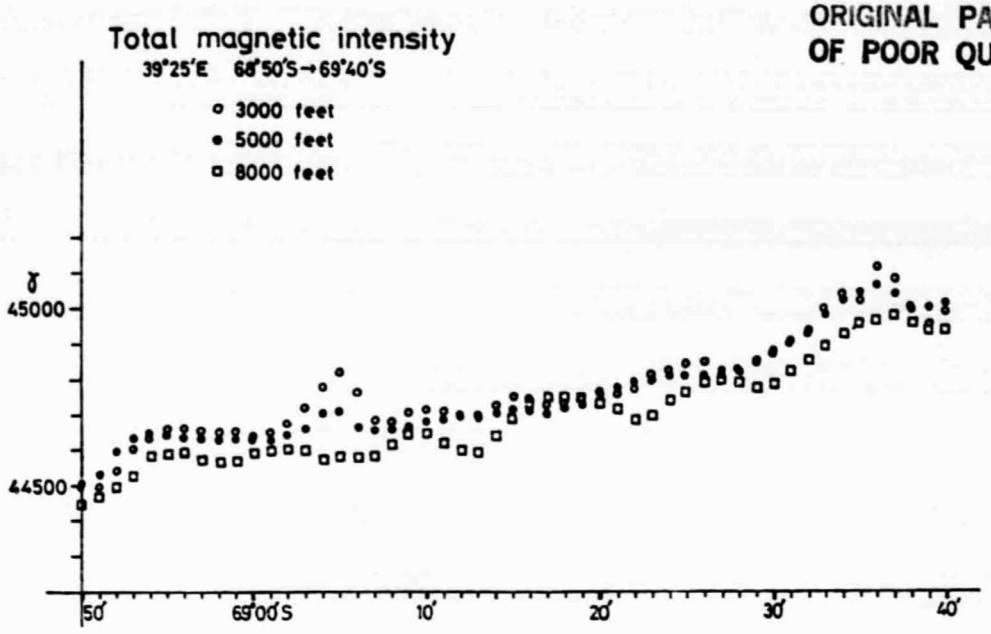

Fig. A3-2. Total intensity obtained by aeromagnetic surveys in the vicinity of Syowa Station, Antarctica, at the altitudes of 3000, 5000 and 8000 feet.

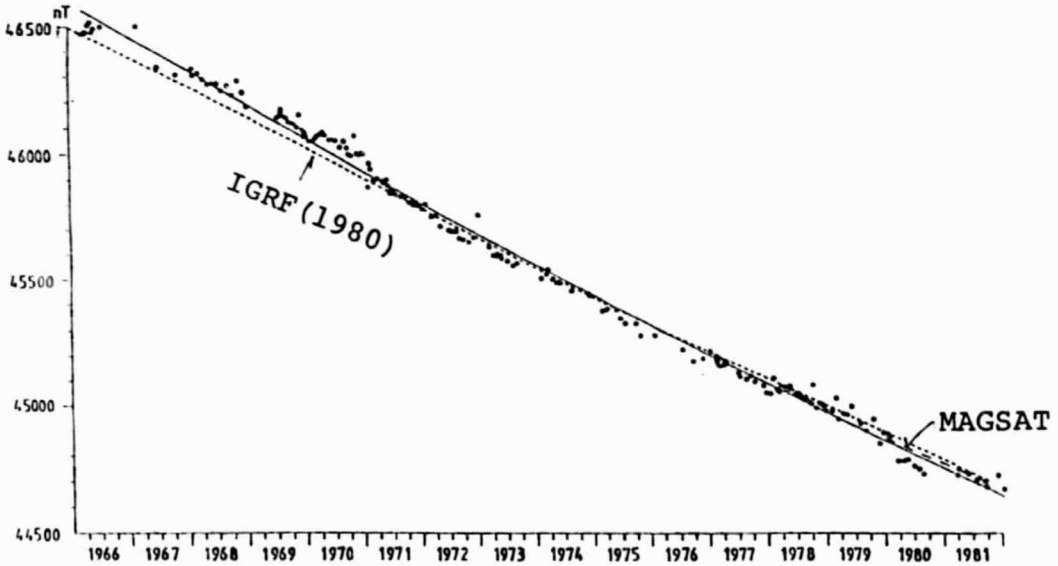

Fig. A3-3. Secular variation in the total intensity of geomagnetic field observed at Syowa Station.

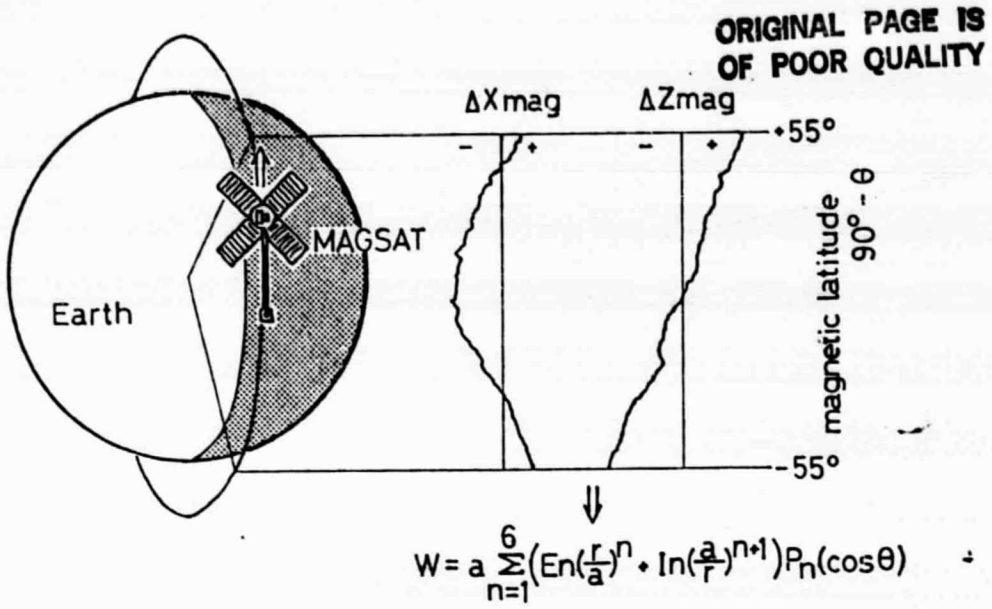

Fig. B1-1. Dependence on magnetic latitude of ΔX_{mag} and ΔZ_{mag} measured by MAGSAT for calculating the magnetic potentials of external (E_n) and internal (I_n) parts by means of the equation shown at the right bottom corner.

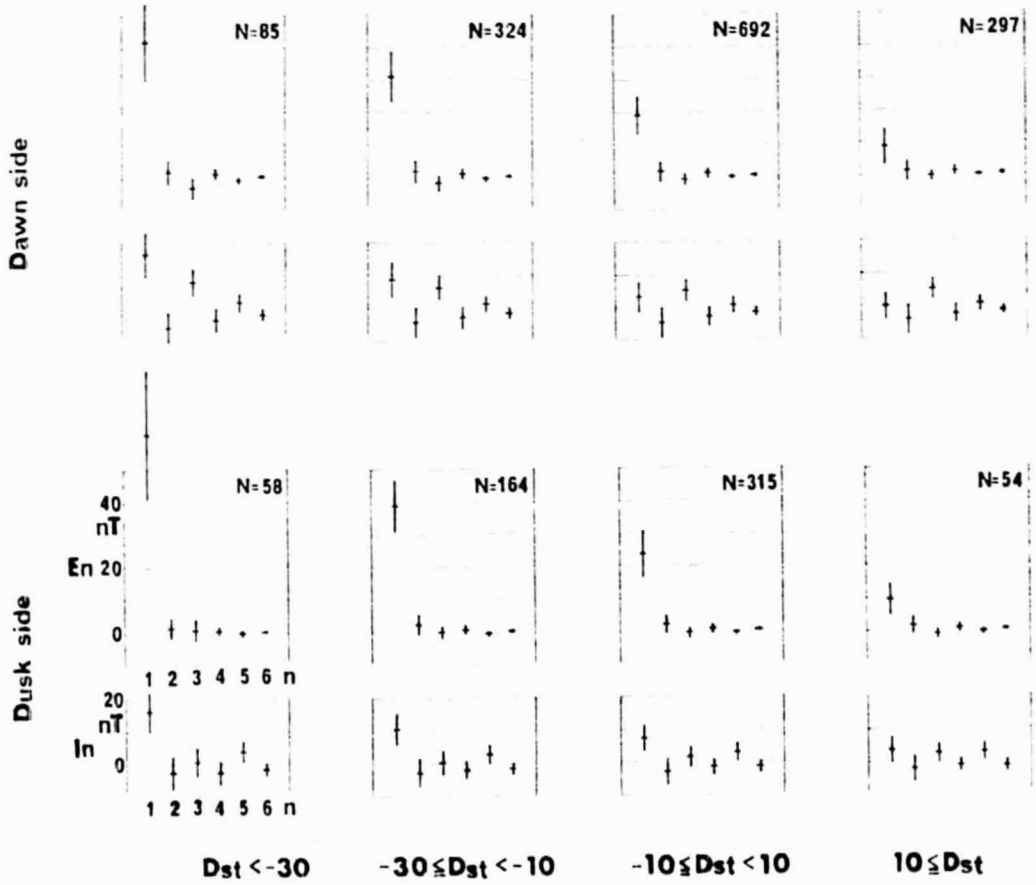

Fig. B1-2. External (E_n) and internal (I_n) coefficient values of the magnetic potential for four classes of Dst values, computed separately for the orbits on the dawn side and the dusk side. Numbers on the right shoulder of each block are those of orbits used for the analysis.

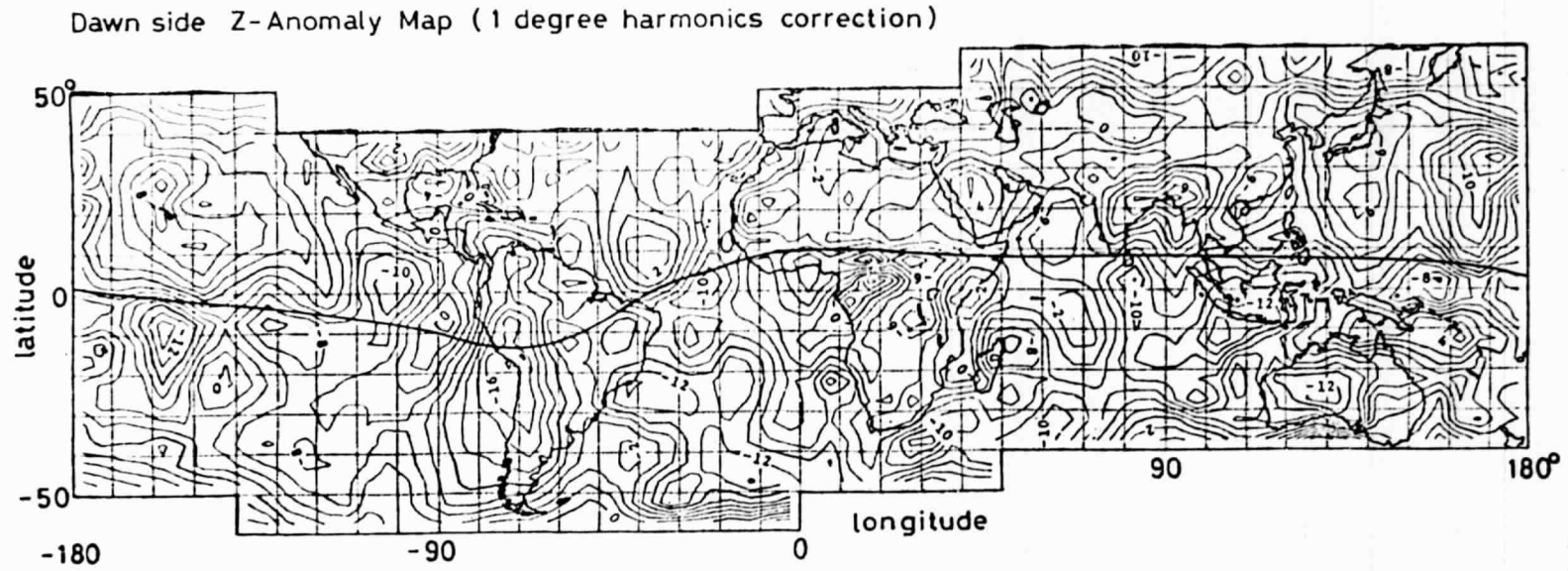

Fig. B1-3(a). Dawn-side Z-anomaly map after removal of MGST(4/81) model field and the magnetospheric and induction fields of the 1st harmonics.

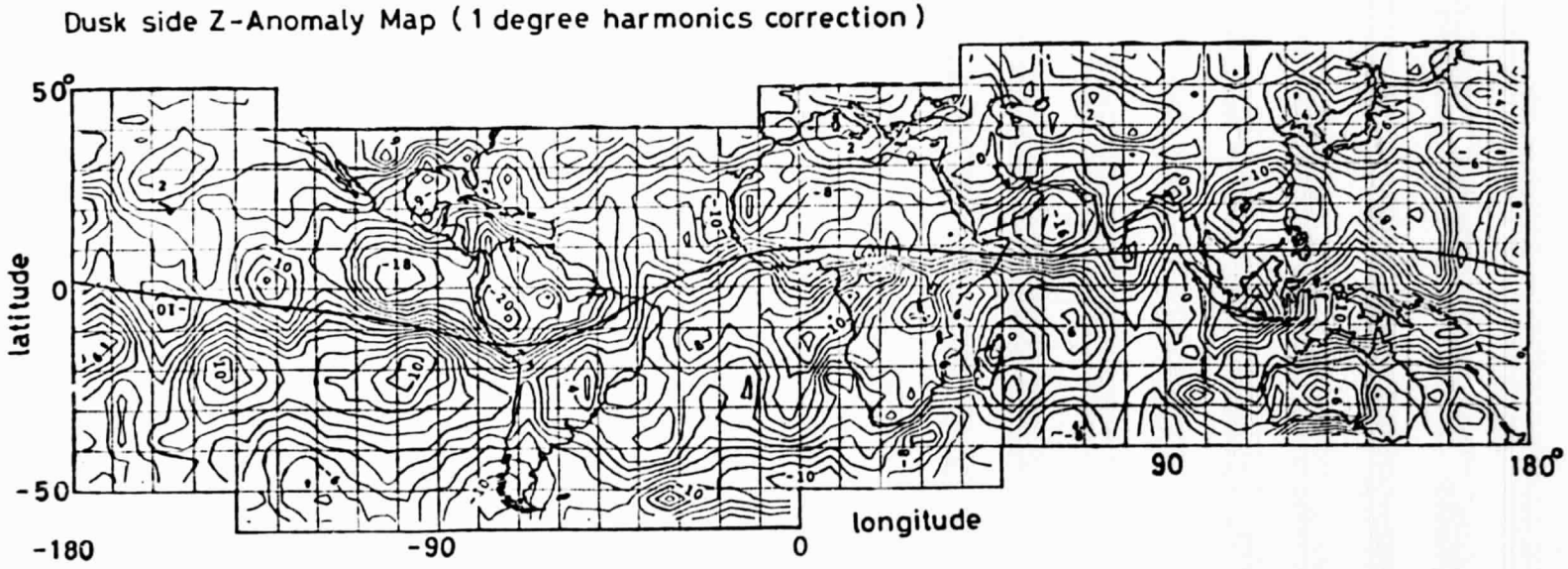

Fig. B1-3(b). Dusk-side Z-anomaly map after removal of MGST(4/81) model field and the magnetospheric and induction fields of the 1st harmonics.

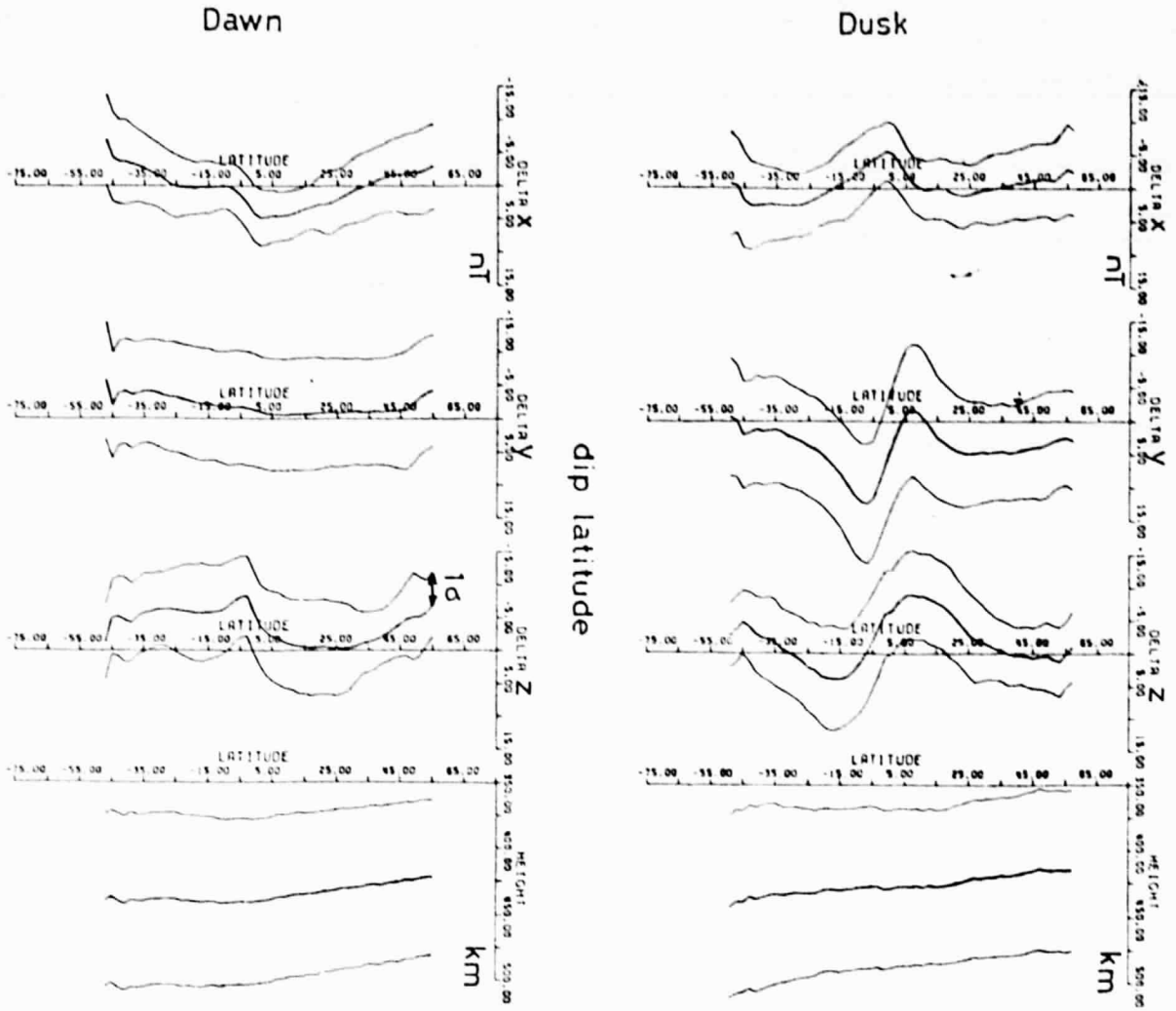

Fig. B1-4. Latitudinal dependence of the "mean ionospheric field" on the dawn and dusk sides, obtained after removal of MGST(4/81) model field and the ring current and induction fields. The thick center curves are the average, and the thin upper and lower curves show the range of standard deviations.

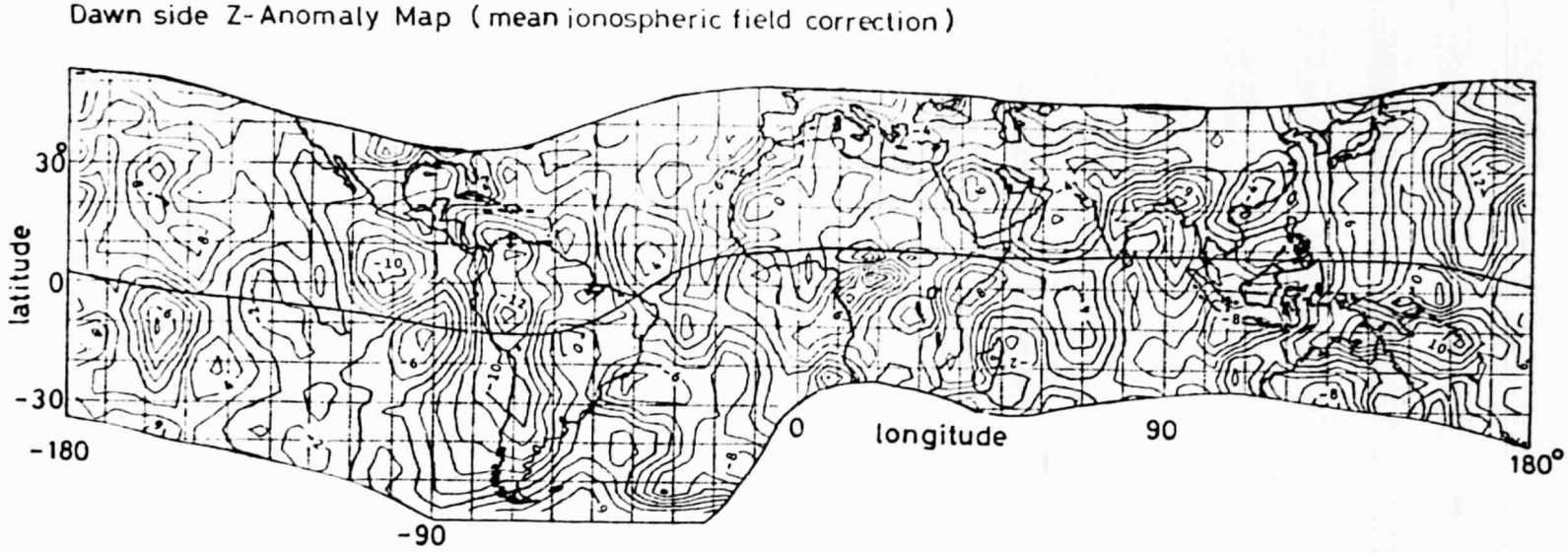

Fig. B1-5(a). Dawn-side Z-anomaly map obtained after subtracting the mean ionospheric field from the map of Fig. B1-3(a). Contour interval is 2 nT.

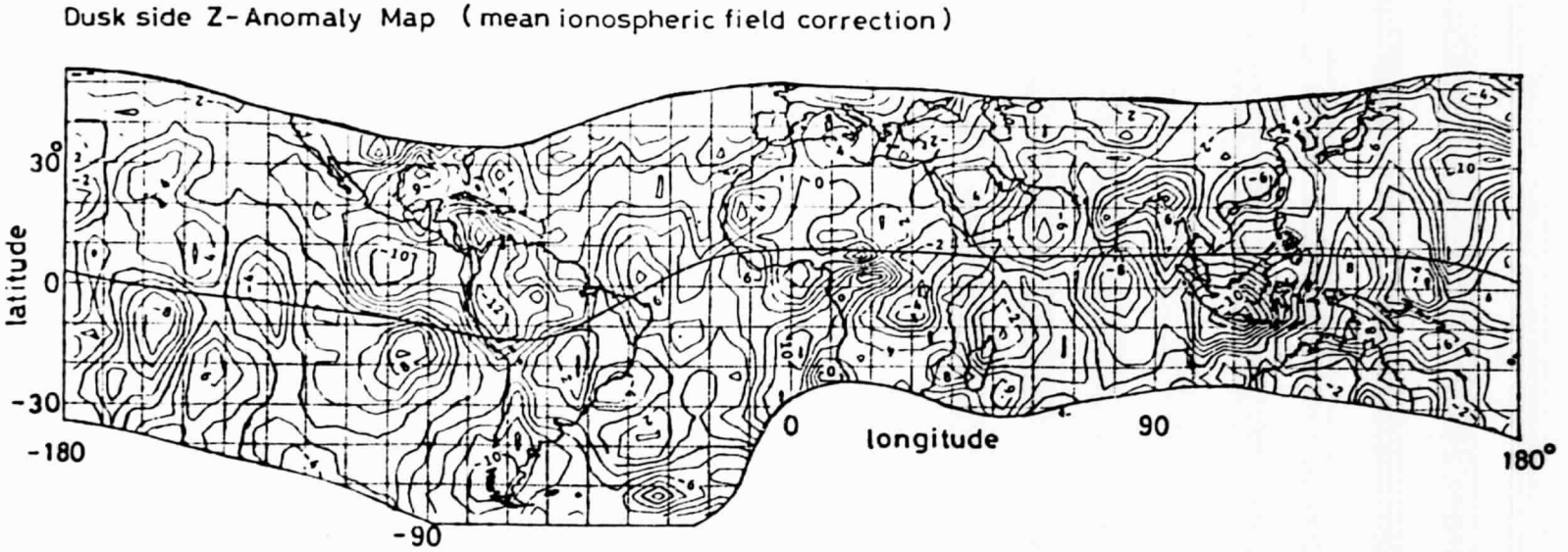

Fig. B1-5(b). Dusk-side Z-anomaly map obtained after subtracting the mean ionospheric field from the map of Fig. B1-3(b). Contour interval is 2 nT.

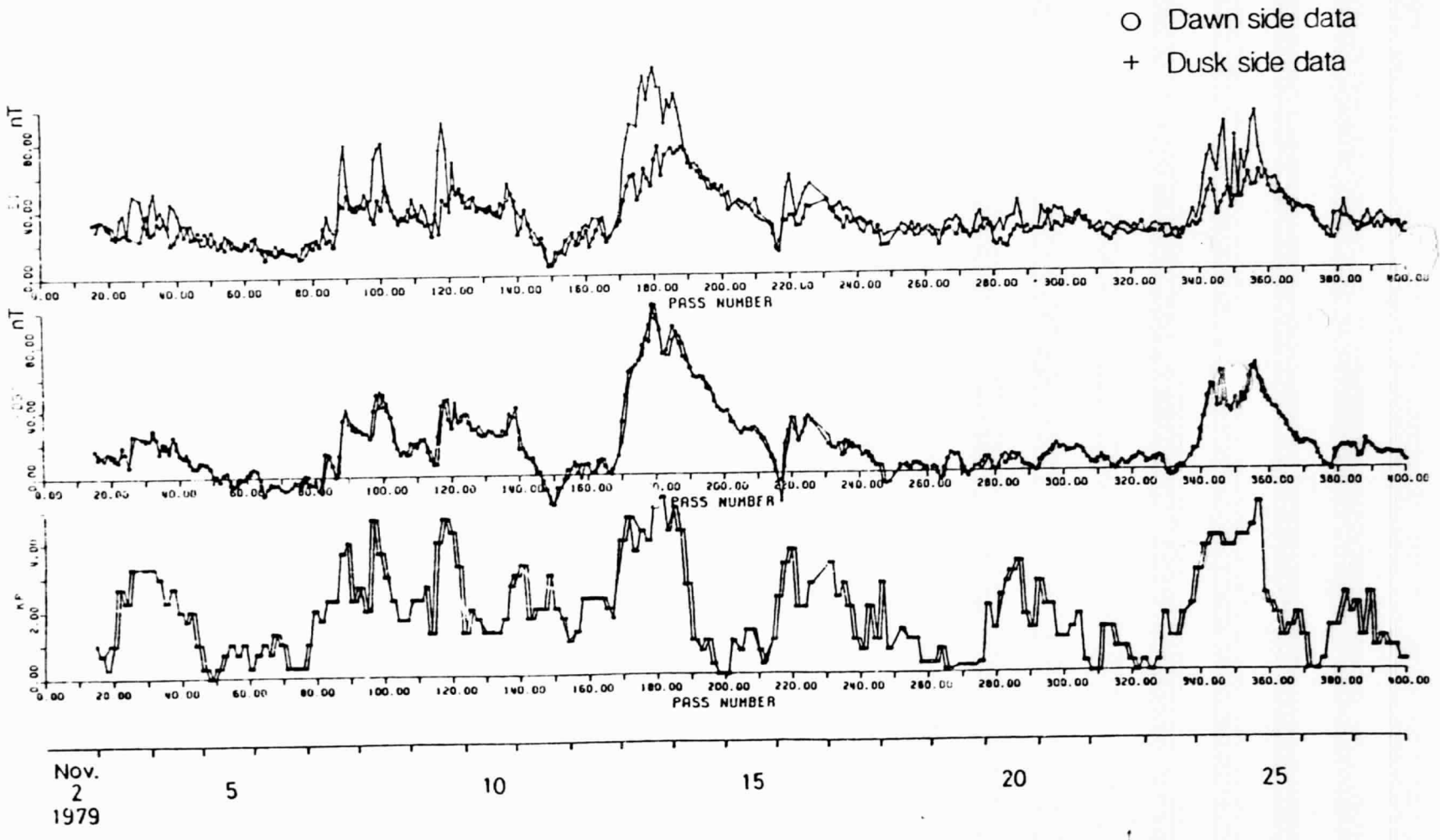

Fig. B1-6. Top: the coefficients E_1 calculated for dawn (o) and dusk (+) paths aginst orbit number. E_1 represents the north-to-south uniform magnetic field parallel to the geomagnetic dipole axis. Middle: Dst values at the time of dawn equator crossing (o) and dusk equator crossing (+) of MAGSAT. Bottom: Kp indices at dawn (o) and dusk(+) equator crossing.

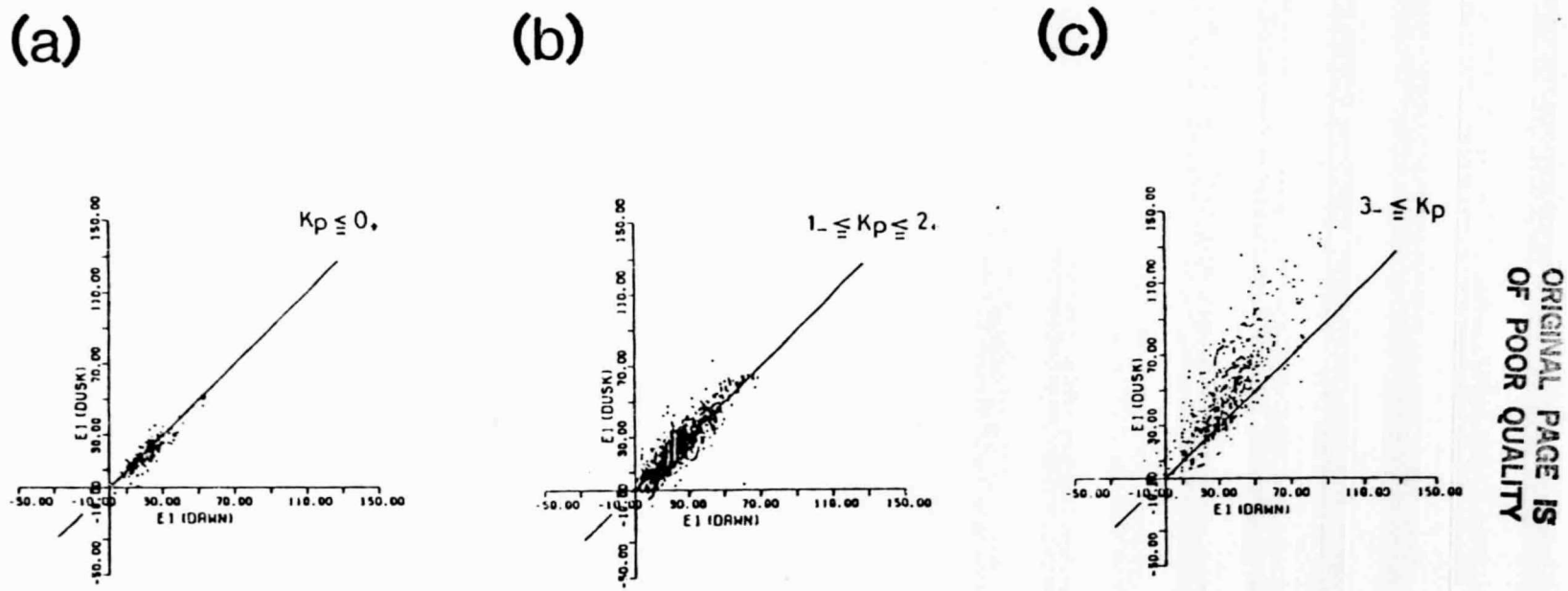

Fig. B1-7. Comparison between E_1 values on the dawn and dusk sides for the Kp ranges of (a) less than or equal to 0_+, (b) between 1_- and 2_+, and (c) equal to or greater than 3_-. The solid lines in the diagrams represent the lines of equal E_1 values on the dawn and dusk sides. For high Kp values, the dawn/dusk asymmetry of E_1 is noticeable.

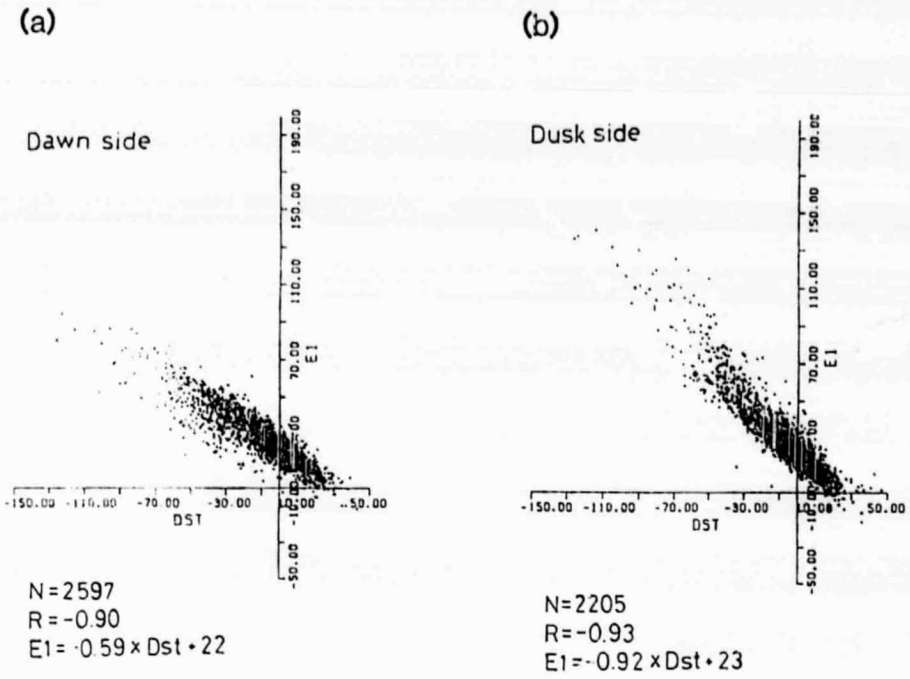

Fig. B1-8. Intensity of the ring current field at the MAGSAT level versus Dst values on the ground, The number of data points (N), correlation coefficient (R) and the best fitted linear function are also shown.

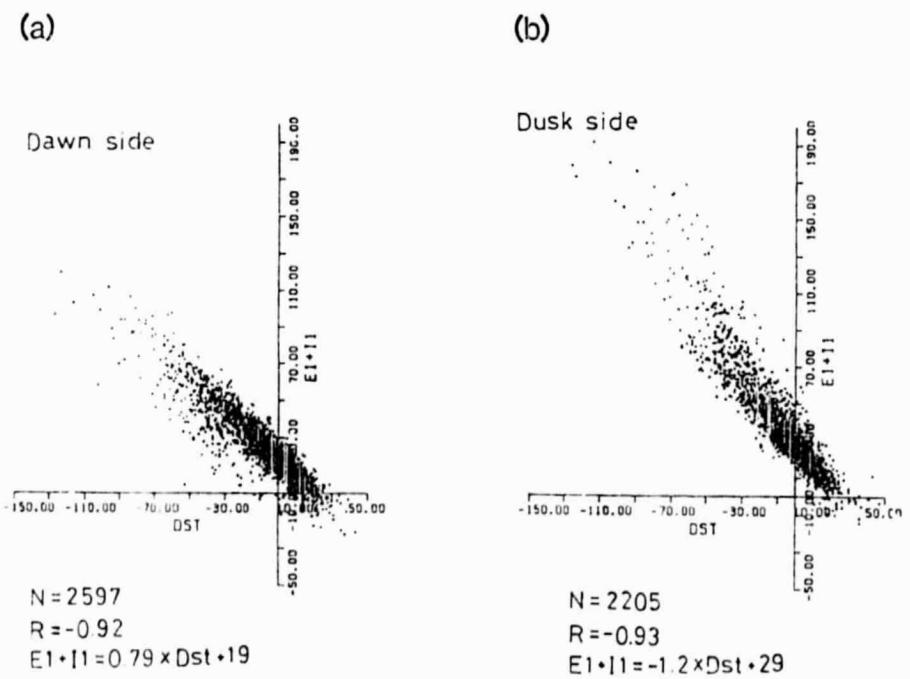

Fig. B1-9. Intensity of the ring current field plus earth's induction and/or ionospheric field at the MAGSAT level versus Dst values on the ground. The number of data points (N), correlation coefficient (R) and the best fitted linear function are also shown.

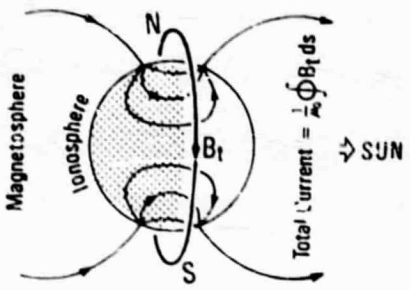

Fig. B1-10. Ampere's theorem applied to a polar orbit satellite.

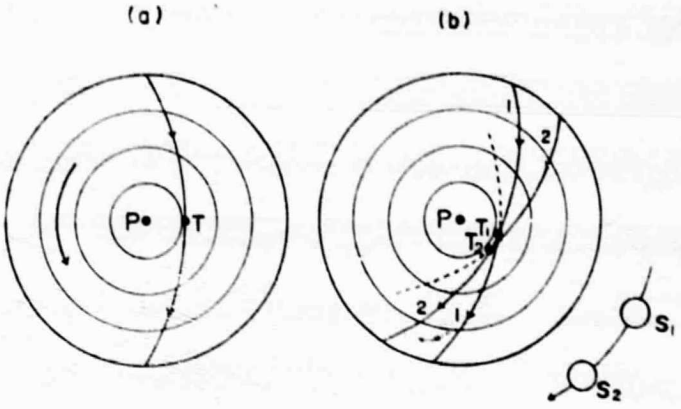

Fig. B1-11. Two methods of B_t-integration: (a) Integral circuit in the sun-earth coordinate system, (b) Loci of satellite orbits projected onto the earth surface.

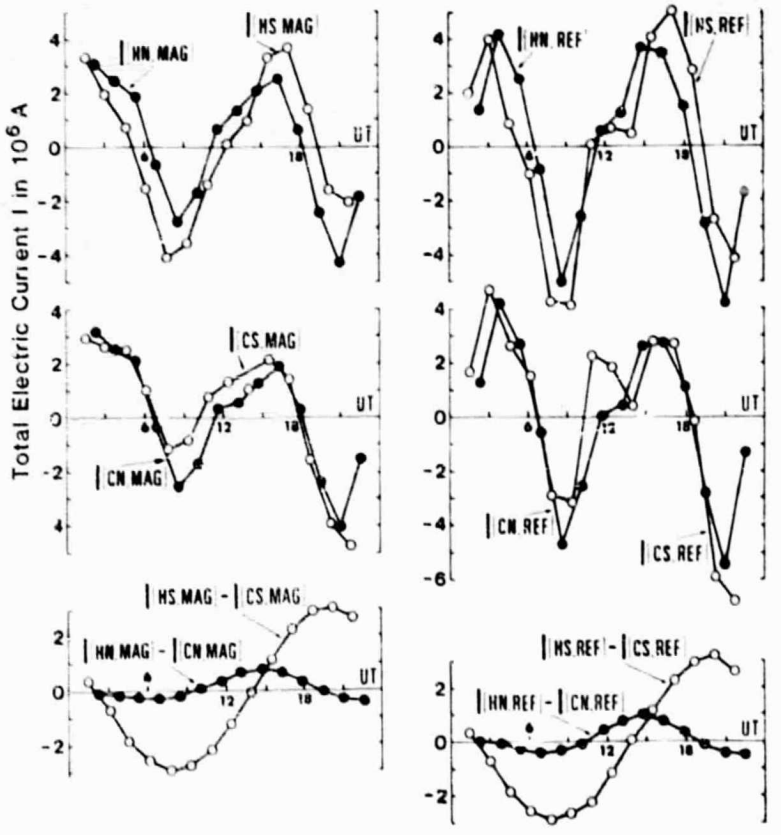

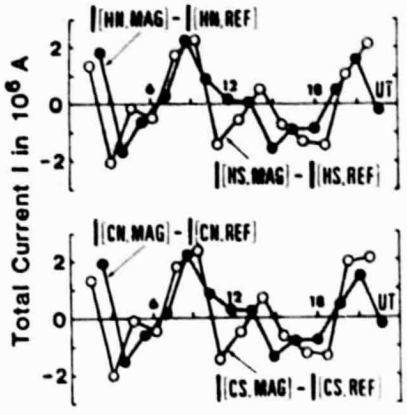

Notation	Data Used	Line-Integration Path along the MAGSAT Orbit
I[HN, MAG]	MAGSAT	from H_1(N) to H_2(N)
I[CN, MAG]	MAGSAT	from C(N) to C(N)
I[HS, MAG]	MAGSAT	from H_1(S) to H_2(S)
I[CS, MAG]	MAGSAT	from C(S) to C(S)
I[HN, REF]	MGST(4/81)	from H_1(N) to H_2(N)
I[CN, REF]	MGST(4/81)	from C(N) to C(N)
I[HS, REF]	MGST(4/81)	from H_1(S) to H_2(S)
I[CS, REF]	MGST(4/81)	from C(S) to C(S)

H in this figure is the same as T in Fig. B1-11, and C denotes the cross-point of two consecutive orbits projected onto the ground. N and S refer to the northern and southern hemispheres.

Fig. B1-12. Results of the numerical line-integration of B_t with the actual MAGSAT data (left diagram), with MGST(4/81) model reference field (middle diagram), and the difference between them (right diagam). These are reproduced from a previous paper (Suzuki and Fukushima, 1982).

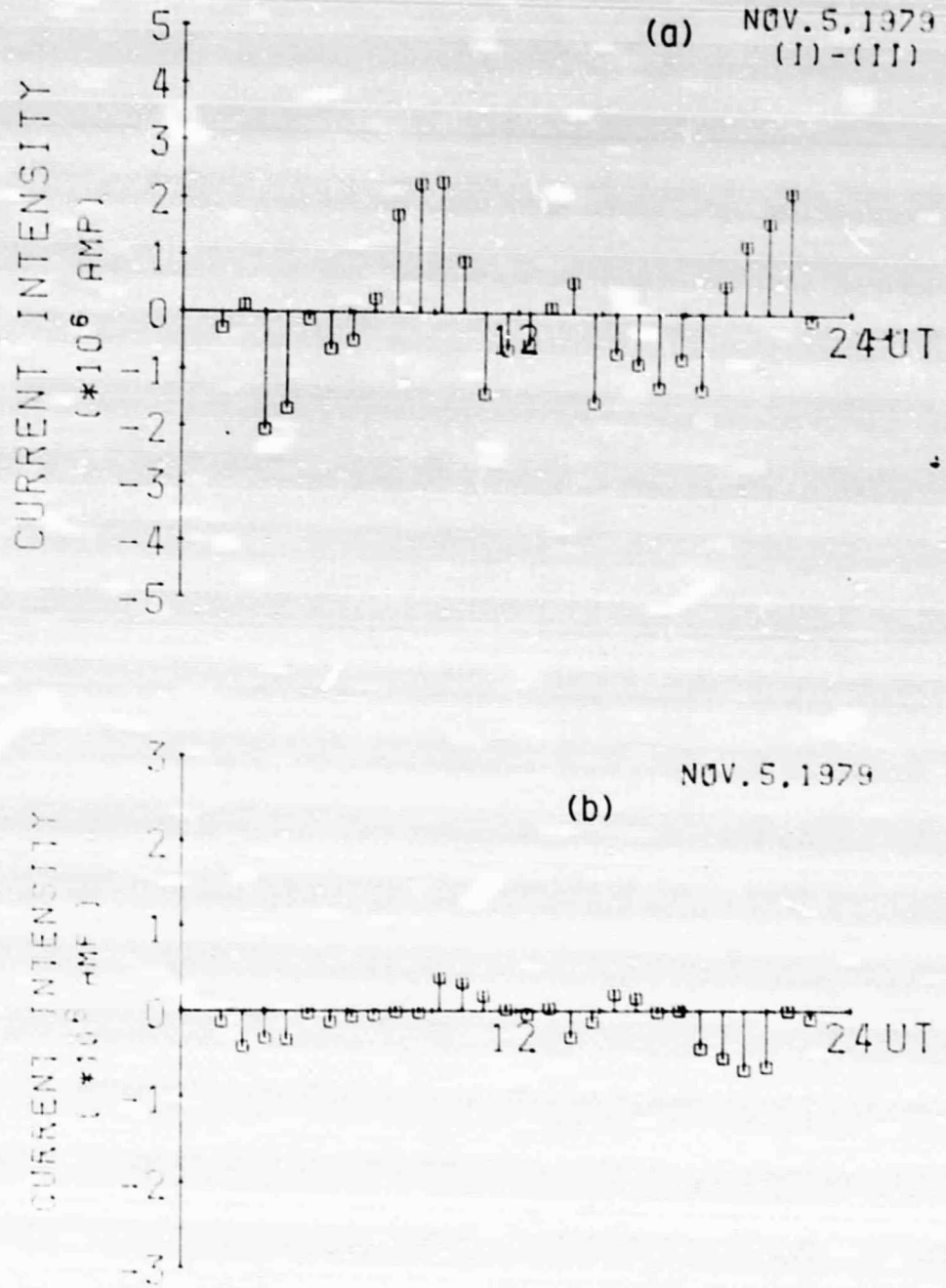

Fig. B1-13. Total intensity of the space current through the plane enclosed by the MAGSAT orbit on a quiet day of November 5, 1979, obtained from the calculation of (a) J(I) - J(II), and (b) J(III). The result in (a) contains an effect of the earth's rotation under the MAGSAT orbit. The effect is eliminated in the calculation in (b).

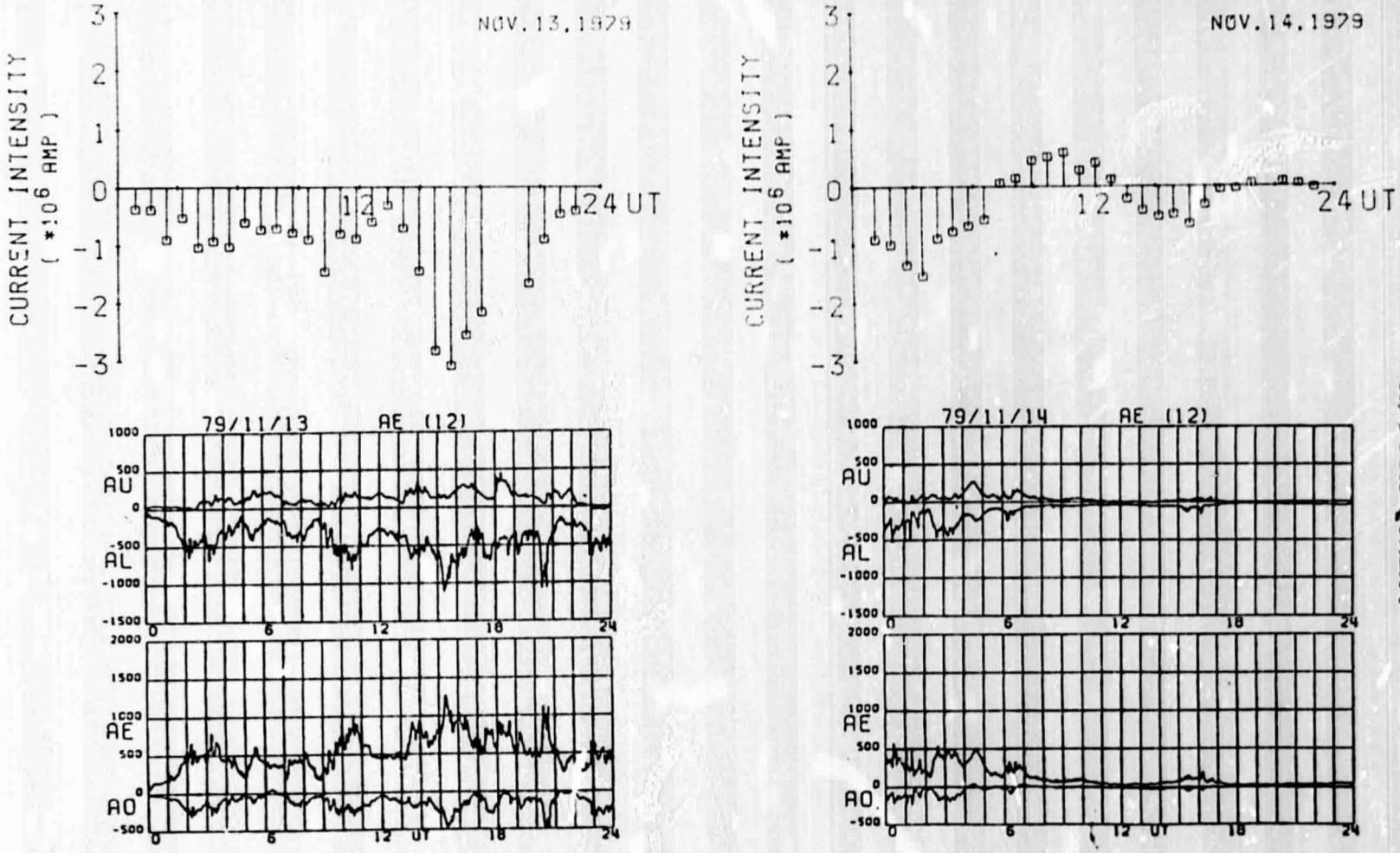

Fig. B1-14. Total current calculated from J(III) and the geomagnetic AE-index on the disturbed days of November 13-14, 1979.

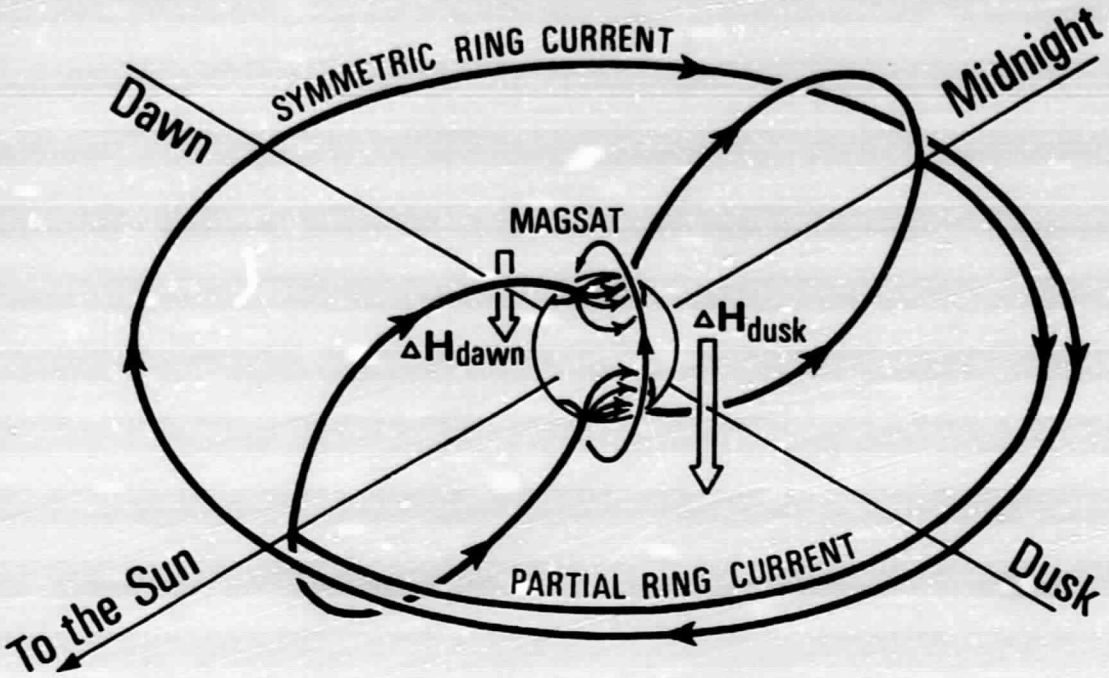

Fig. B1-15. A schematic model model of the ring current during magnetic disturbance with partial ring current connected with anti-sunward field-aligned currents into and out of the ionosphere. This model explaing the dawn/dusk asymmetry of ΔH in low latitudes and the space current under the MAGSAT orbit.

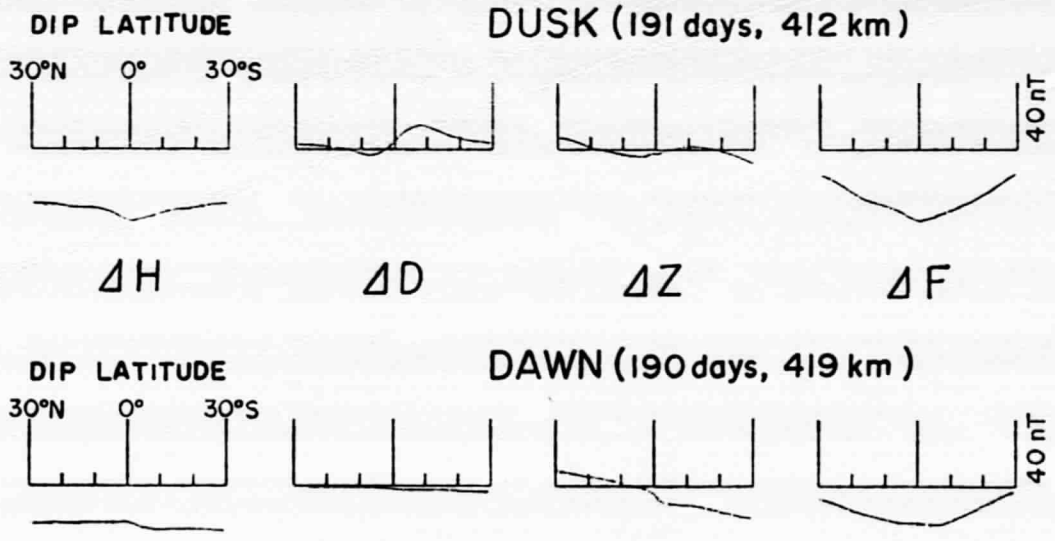

Fig. B1-16. Average profile of the residuals (ΔH, ΔD, ΔZ, and ΔF) from the main field at low latitudes for all days of the MAGSAT observation period at the dusk and dawn meridians, where the number of days used and the mean altitude of MAGSAT are shown in parentheses.

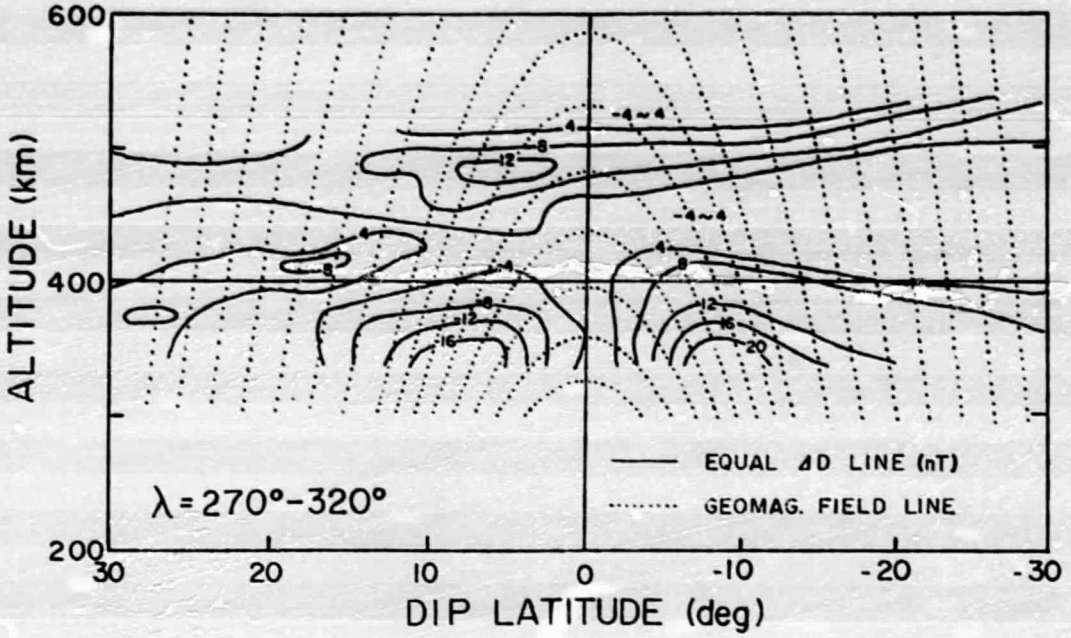

Fig. B1-17. Distribution of ΔD in the average meridian plane (λ = 270°-320°), where the equal ΔD lines (in nT) and the geomagnetic field lines are shown by full and dotted lines, respectively.

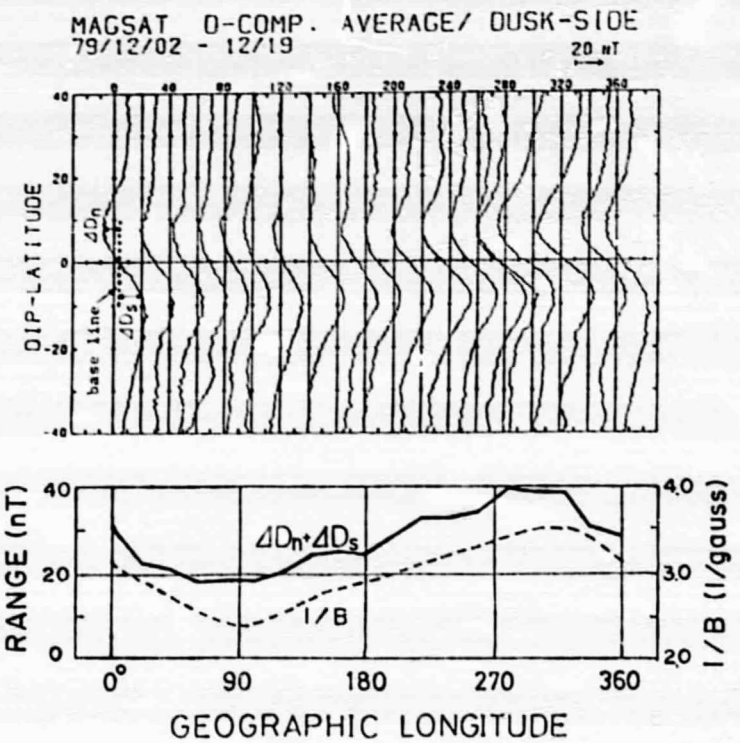

Fig. B1-18. Longitudinal dependence of ΔD averaged over 18 days on the dusk side (top), and that of the total range ($\Delta D_n + \Delta D_s$) together with the values of 1/B (bottom).

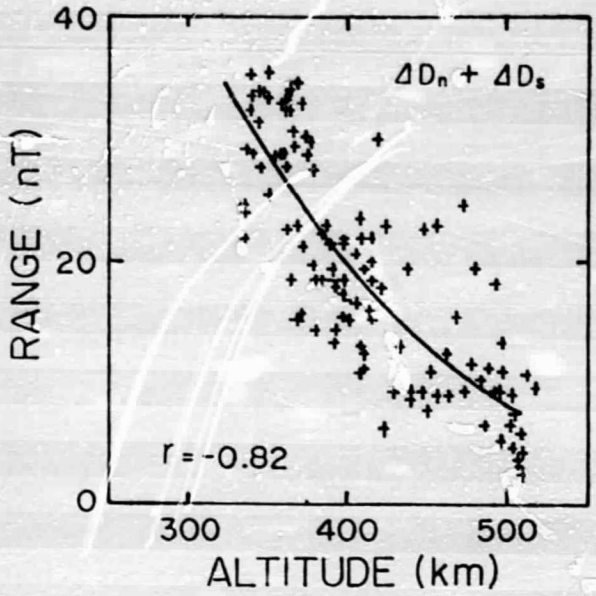

Fig. B1-19. Variation of the ΔD range with altitude, where the full line shows a least-square fit and r is the correlation coefficient.

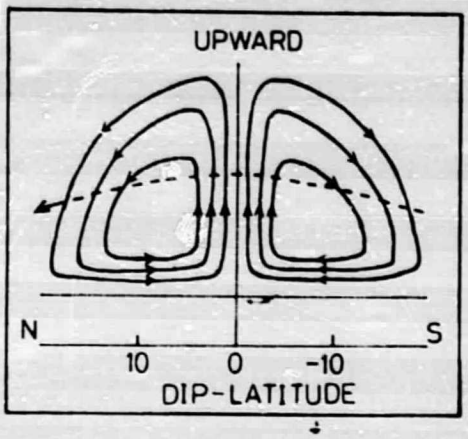

Fig. B1-20. A model for the interpretation of the observed peculiar ΔD on the dusk side.

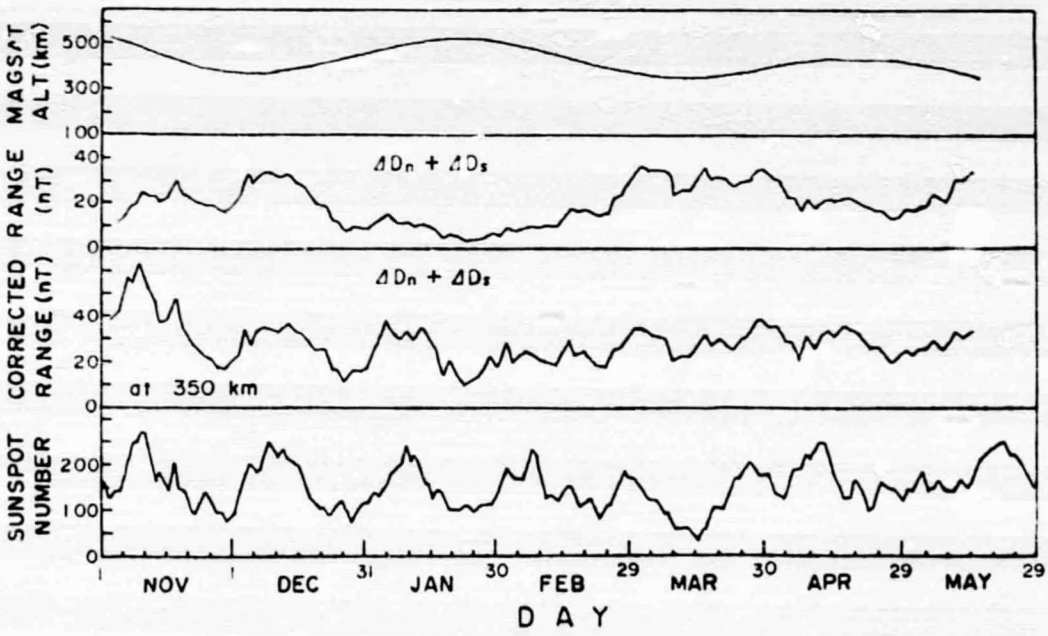

Fig. B1-21. Variation with time of the MAGSAT altitude, ΔD range, corrected range of ΔD at 350 km altitude, and sunspot number.

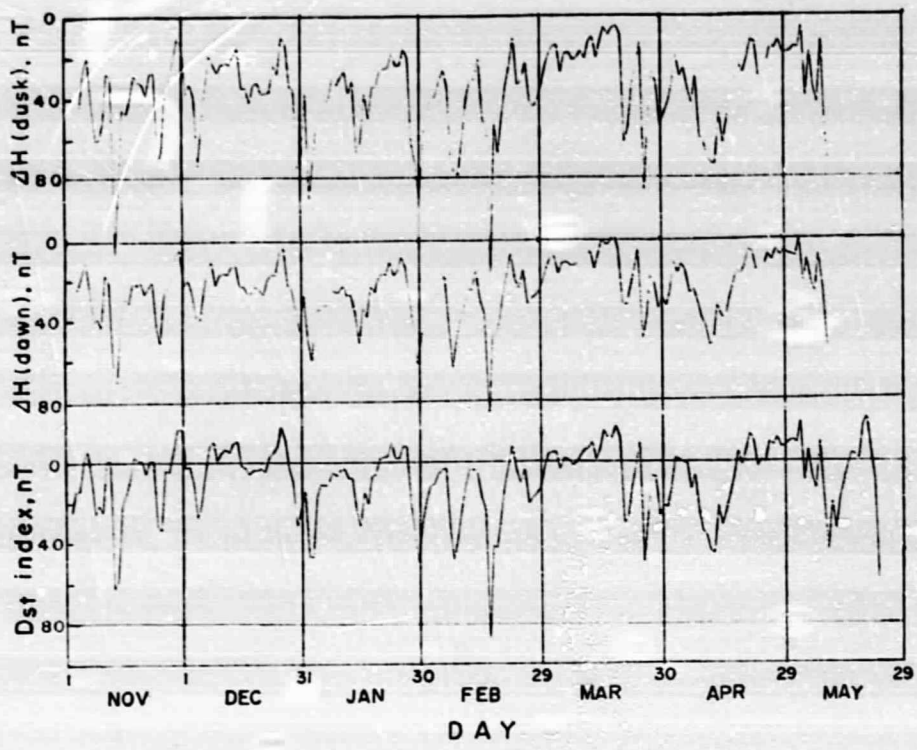

Fig. B1-22. Variation with time of ΔH (dusk) and ΔH (dawn) and the Dst index.

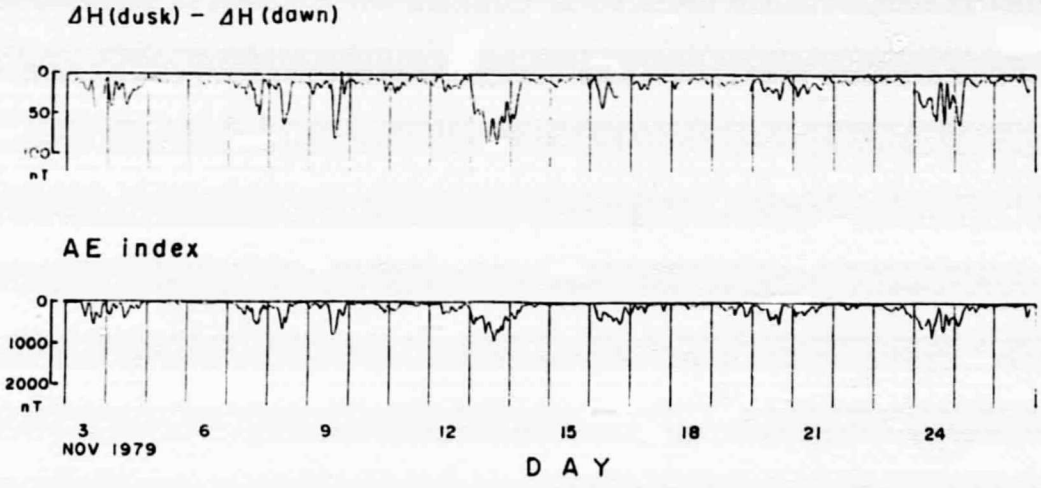

Fig. B1-23. Variation with time of the difference in ΔH at dusk and dawn, and the AE index.

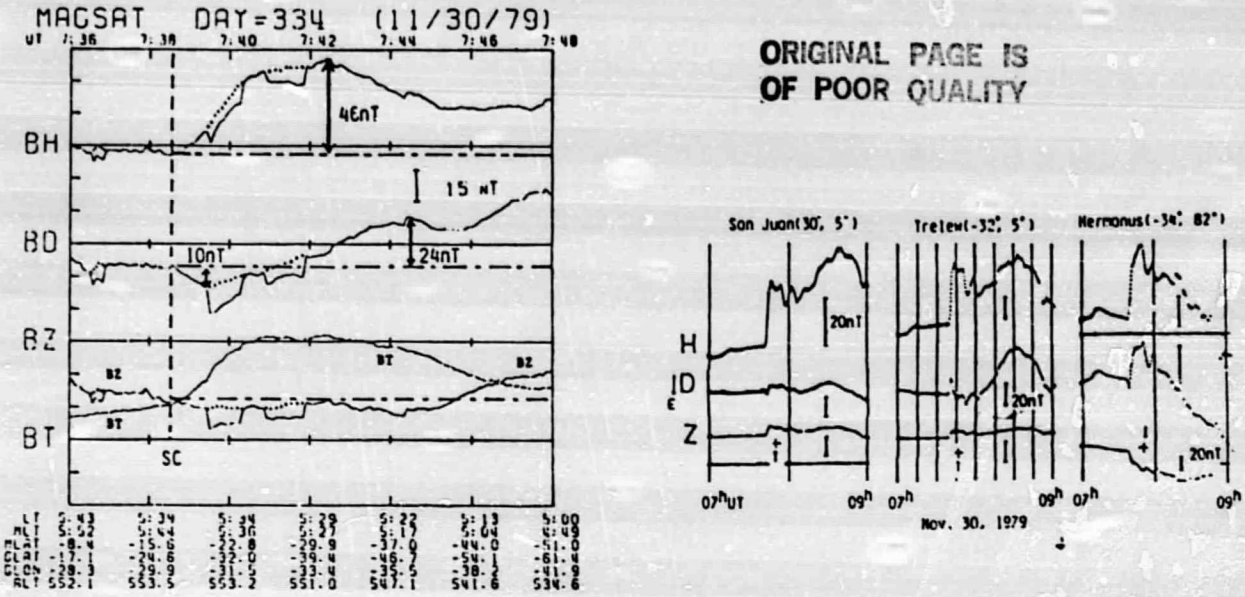

Fig. B1-24. The time variation of the three components and the total force (all are the deviations from MGST(6/80) model field) observed by MAGSAT and the normal-run magnetograms from 3 stations near the MAGSAT position at the time of SC on November 30, 1979. Discontinuous jumps in MAGSAT data due to the attitude inaccuracy are corrected by dotted lines.

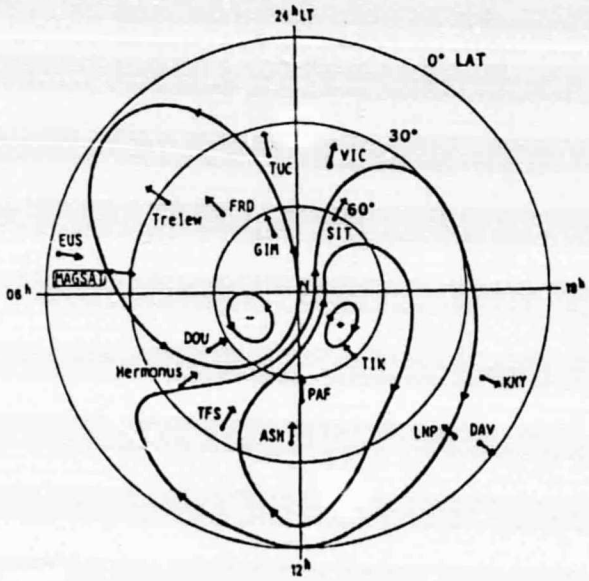

Fig. B1-25. Ionospheric current system for the averaged PRI in the northern hemisphere in the geomagnetic latitude - local time coordinates. Arrows indicate the direction of the N-S component of an assumed ionospheric current for PRI observed by MAGSAT and at ground stations. Positions of MAGSAT and three southern hemisphere stations (Trelew, Hermanus and Port aux Francais) are projected to the conjugate points in the northern hemisphere.

ORIGINAL PAGE IS
OF POOR QUALITY

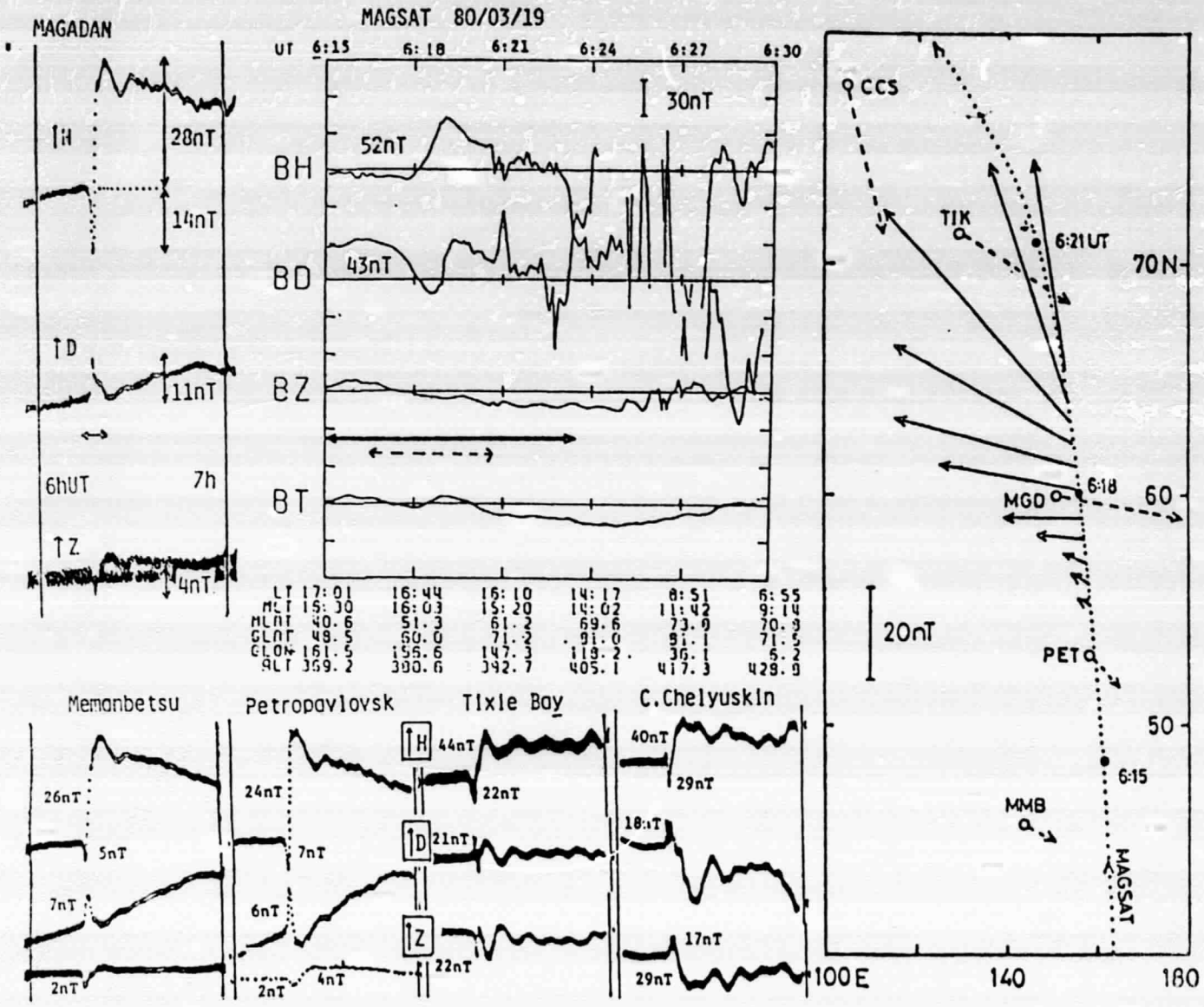

Fig. B1-26. SC event on March 19, 1980. Broken arrows in the right panel indicate horizontal magnetic vectors of the PI of SC observed at ground stations. Solid arrows show the successive variation in the horizontal magnetic vector along the MAGSAT orbit for the time interval shown by a dashed horizontal bar in the central panel. Solid horizontal bars in the central and left panels indicate an equal time interval.

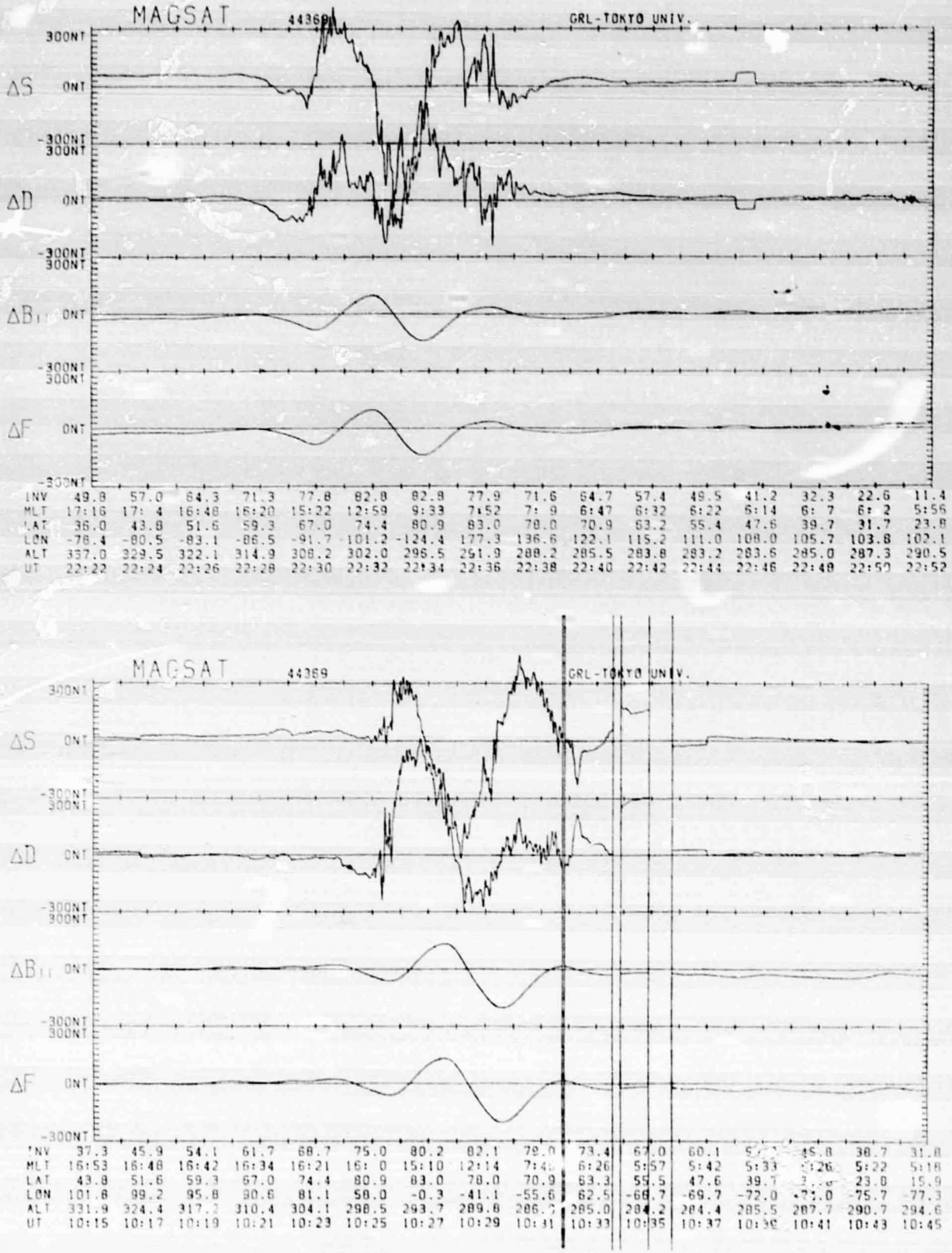

Fig. B2-1. Geomagnetic vector residuals separated into ΔS (perturbation transverse to the main geomagnetic field and directed toward the sun), ΔD (perturbation transverse to the main field and in the dusk-to-dawn direction) and $\Delta B_{\parallel}$ (perturbation parallel to the main field), obtained from the MAGSAT data for two paths over the northern hemisphere on a very quiet day of May 10, 1980 (UT 1015-1045 and 2222-2252).

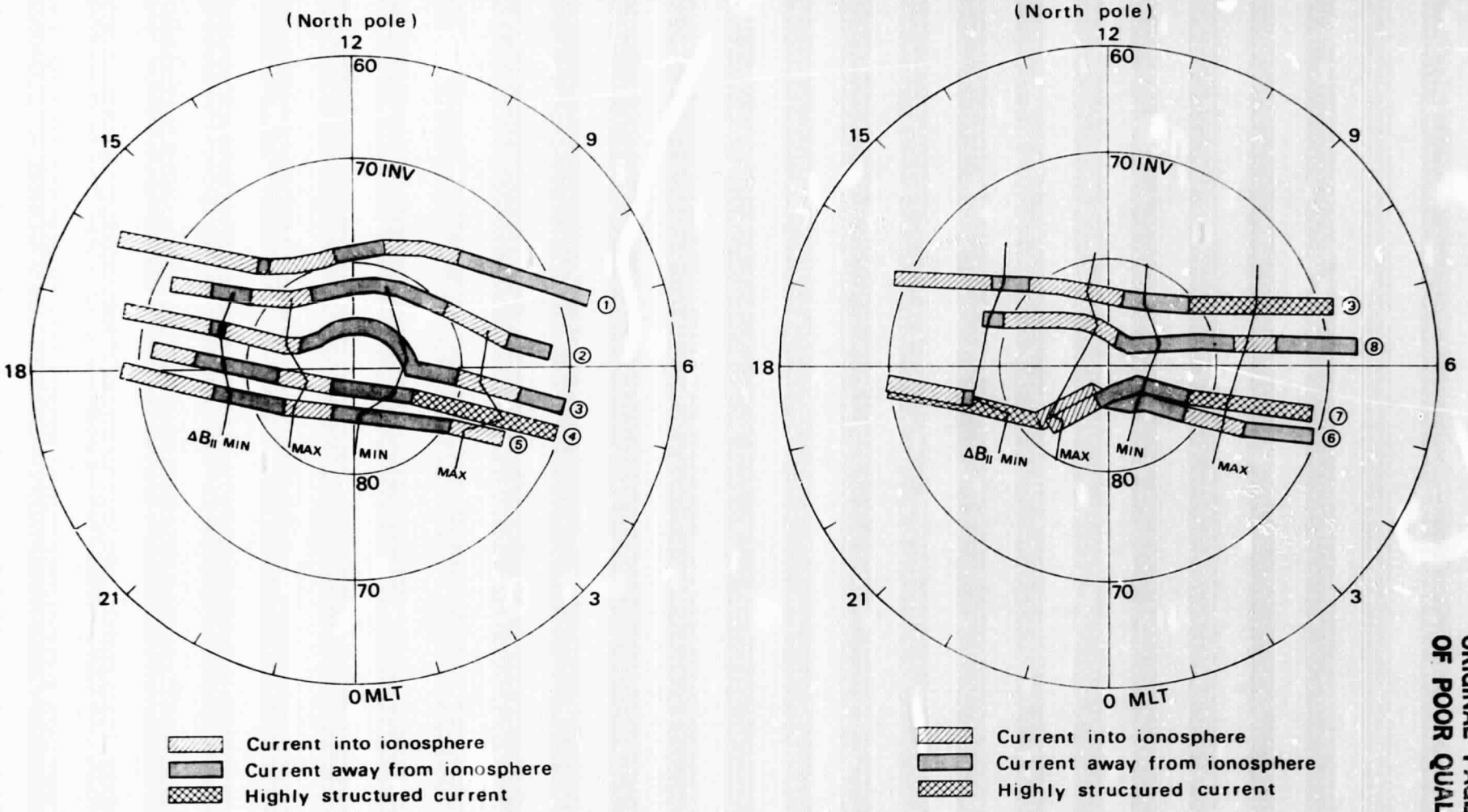

Fig. B2-2. Spatial distribution of field-aligned currents and maximum-minimum of $\Delta B_{\parallel}$ over the northern polar region. The left diagram is for 5 consecutive paths during 0851-1507 UT on May 10, 1980, and the right diagram for 4 consecutive paths during 1626-2239 UT on the same day.

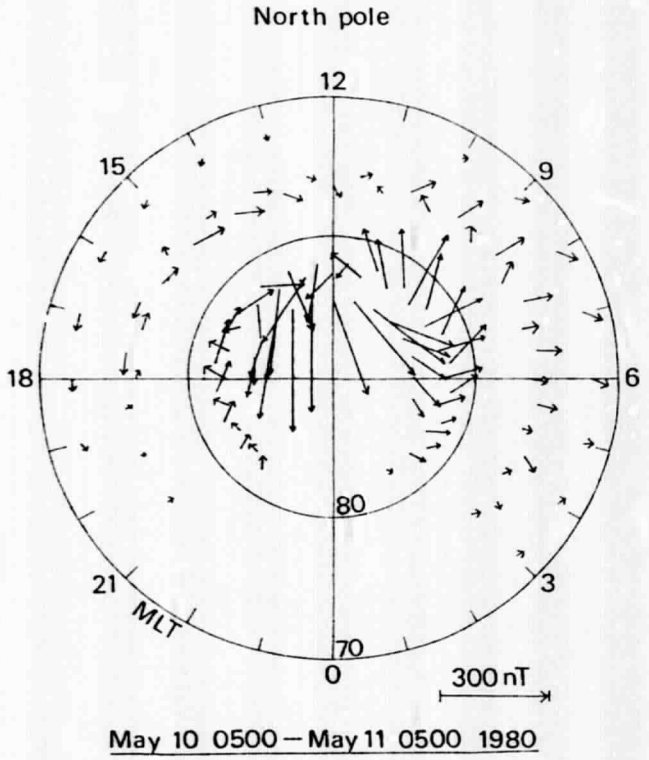

Fig. B2-3. Spatial distribution of equivalent current vectors derived from horizontal magnetic disturbance vectors at Thule (84.3°), Resolute (82.6°), Mould Bay (81.9°), Cambridge Bay (76.5°), Godhavn (75.8°) and Baker Lake (72.2°). The base line values were defined as average values between 2100 and 0300 MLT at each station.

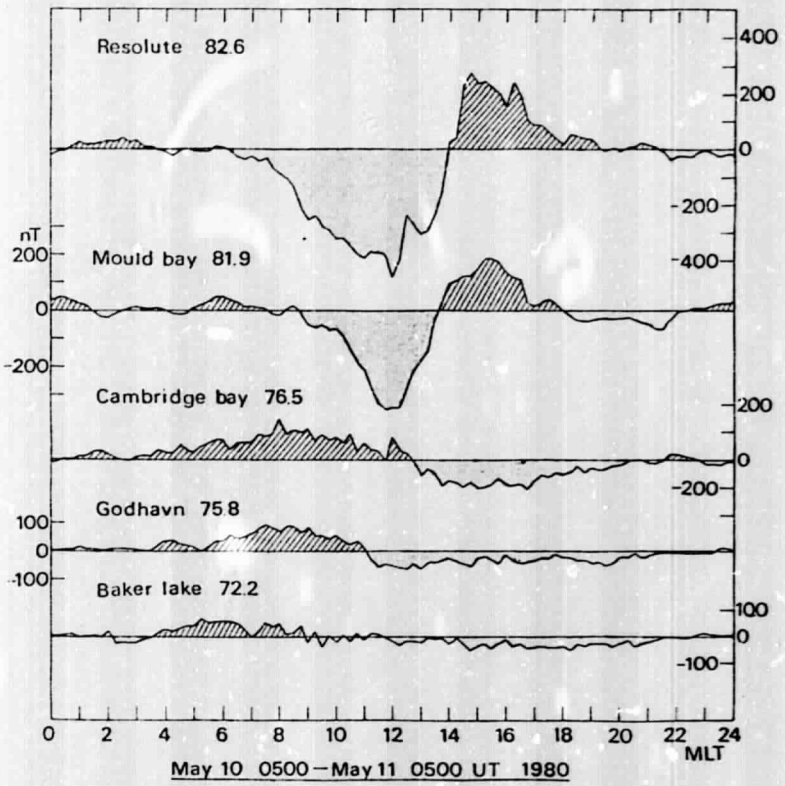

Fig. B2-4. Geomagnetic perturbations of ΔZ at 5 high-latitude stations. The eccentric dipole latitude of each station is indicated after the observatory name.